Cooperative Non-Orthogonal Multiple Access with Simultaneous Wireless Information and Power Transfer

Yuanwei Liu, *Student Member, IEEE,* Zhiguo Ding, *Member, IEEE,*
Maged Elkashlan, *Member, IEEE,* and H. Vincent Poor, *Fellow, IEEE*

***Abstract*—In this paper, the application of simultaneous wireless information and power transfer (SWIPT) to non-orthogonal multiple access (NOMA) networks in which users are spatially randomly located is investigated. A new cooperative SWIPT NOMA protocol is proposed, in which near NOMA users that are close to the source act as energy harvesting relays to help far NOMA users. Since the locations of users have a significant impact on the performance, three user selection schemes based on the user distances from the base station are proposed. To characterize the performance of the proposed selection schemes, closed-form expressions for the outage probability and system throughput are derived. These analytical results demonstrate that the use of SWIPT will not jeopardize the diversity gain compared to the conventional NOMA. The proposed results confirm that the opportunistic use of node locations for user selection can achieve low outage probability and deliver superior throughput in comparison to the random selection scheme.**

***Index Terms*—Non-orthogonal multiple access, simultaneous wireless information and power transfer, stochastic geometry, user selection**

I. Introduction

Non-orthogonal muliple access (NOMA) is an effective solution to improve spectral efficiency and has recently received significant attention for its promising application in fifth generation (5G) networks [1]. The key idea of NOMA is to realize multiple access (MA) in the power domain which is fundamentally different from conventional orthogonal MA technologies (e.g., time/frequency/code division MA). The motivation behind this approach lies in the fact that NOMA can use spectrum more efficiently by opportunistically exploring users' channel conditions [2]. In [3], the authors investigated the performance of a downlink NOMA scheme with randomly deployed users. An uplink NOMA transmission scheme was proposed in [4], and its performance was evaluated systematically. In [2], the impact of user pairing was characterized by analyzing the sum rates in two NOMA systems, namely, fixed power allocation NOMA and cognitive radio inspired NOMA. In [5], a new cooperative NOMA scheme was proposed and analyzed in terms of outage probability and diversity gain.

In addition to improving spectral efficiency which is the motivation of NOMA, another key objective of future 5G networks is to maximize energy efficiency. Simultaneous wireless information and power transfer (SWIPT), which was initially proposed in [6], has rekindled the interest of researchers to explore more energy efficient networks. In [6], it was assumed that both information and energy could be extracted from the same radio frequency signals at the same time, which does not hold in practice. Motivated by this issue, two practical receiver architectures, namely time switching (TS) receiver and power splitting (PS) receiver, were proposed in a multi-input and multi-output (MIMO) system in [7]. Since point-to-point communication systems with SWIPT are well established in the existing literature, recent research on SWIPT has focused on two common cooperative relaying systems: amplify-and-forward (AF) and decode-and-forward (DF). On the one hand, for AF relaying, a TS-based relaying protocol and a PS-based relaying protocol were proposed in [8]. On the other hand, for DF relaying, a new antenna switching SWIPT protocol was proposed in [9] to lower the implementation complexity. In [10], the application of SWIPT to DF cooperative networks with randomly deployed relays was investigated using stochastic geometry in a cooperative scenario with multiple source nodes and a single destination. A scenario in which multiple source-destination pairs are randomly deployed and communicate with each other via a single energy harvesting relay was considered in [11].

A. Motivation and Contributions

One important advantage of the NOMA concept is that it can squeeze a user with better channel conditions into a channel that is occupied by a user with worse channel conditions [2]. For example, consider a downlink scenario in which there are two groups of users: 1) near users, which are close to the base station (BS) and have better channel conditions; and 2) far users, which are close to the edge of the cell controlled by the BS and therefore have worse channel conditions. While the spectral efficiency of NOMA is superior compared to orthogonal MA, the fact that the near users co-exist with the far users causes performance degradation to the far users. In order to improve the reliability

Y. Liu and M. Elkashlan are with the School of Electronic Engineering and Computer Science, Queen Mary University of London, London E1 4NS, UK. (email:{yuanwei.liu, maged.elkashlan}@qmul.ac.uk).

Z. Ding and H. V. Poor are with the Department of Electrical Engineering, Princeton University, Princeton, NJ 08544, USA. (e-mail: poor@princeton.edu). Z. Ding is also with the School of Computing and Communications, Lancaster University, LA1 4WA, UK. (e-mail: z.ding@lancaster.ac.uk).

This research was supported in part by the UK EPSRC under grant number EP/L025272/1 and the U.S. National Science Foundation under Grant EECS-1343210.

of the far users, an efficient method was proposed in [5] by applying cooperative transmission to NOMA. The key idea of this cooperative NOMA scheme is that the users that are close to the BS are used as relays to help the far users with poor channel conditions. The advantage of implementing cooperative transmission in NOMA systems is that successive interference cancelation is used at the near users and hence the information of the far users is known by these near users. In this case, it is natural to consider the use of the near users as DF relays to transmit information to the far users.

In this paper, we consider this setting, but with the additional feature that the near users are energy constrained and hence harvest energy from their received RF signals. To improve the reliability of the far NOMA users without draining the near users' batteries, we consider the application of SWIPT to NOMA, where SWIPT is performed at the near NOMA users. Therefore, the aforementioned two communication concepts, cooperative NOMA and SWIPT, can be naturally linked together, and a new spectrally and energy efficient wireless multiple access protocol, namely, the cooperative SWIPT NOMA protocol, is proposed in this paper. In order to investigate the impact of the locations of randomly deployed users on the performance of the proposed protocol, tools from stochastic geometry are used. Particularly, users are spatially randomly deployed in two groups via homogeneous Poisson point processes (PPPs). Here, the near users are grouped together and randomly deployed in an area close to the BS. The far users are in the other group and are deployed close to the edge of the cell controlled by the BS.

Since NOMA is co-channel interference limited, it is important to combine NOMA with conventional orthogonal MA technologies and realize a new hybrid MA network. For example, we can first group users in pairs to perform NOMA, and then use conventional time/frequency/code division MA to serve the different user pairs. Note that this hybrid MA scheme can effectively reduce the system complexity since fewer users are grouped together for the implementation of NOMA. Based on the proposed protocol and the considered stochastic geometric model, a natural question arises: which near NOMA user should help which far NOMA user? To investigate the performance of one pair of selected NOMA users, three opportunistic user selection schemes are proposed, based on locations of users to perform NOMA as follows: 1) random near user and random far user (RNRF) selection, where both the near and far users are randomly selected from the two groups; 2) nearest near user and nearest far user (NNNF) selection, where a near user and a far user closest to the BS are selected from the two groups; and 3) nearest near user and farthest far user (NNFF) selection, where a near user which is closest to the BS is selected and a far user which is farthest from the BS is selected. The insights obtained from these opportunistic user selection schemes provide guidance for the design of dynamic user clustering algorithms, a topic beyond the scope of the paper.

The primary contributions of our paper are summarized as follows.

- We propose a new SWIPT NOMA protocol to improve the reliability of the far users with the help of the near users without consuming extra energy. With this in mind, three user selection schemes are proposed by opportunistically taking into account the users' locations.
- We derive closed-form expressions for the outage probability at the near and far users, when considering the three proposed user selection schemes. In addition, we analyze the delay-sensitive throughput based on the outage probabilities of the near and far users.
- We derive the diversity gain of the three proposed selection schemes for the near and far users. We conclude that all three schemes have the same diversity order. For the far users, it is worth noting that the diversity gain of the proposed cooperative SWIPT NOMA is the same as that of a conventional cooperative network without radio frequency energy harvesting.
- Comparing RNRF, NNNF, and NNFF, we confirm that NNNF achieves the lowest outage probability and the highest throughput for both the near and far users.

B. Organization

The rest of the paper is organized as follows. In Section II, the network model for studying cooperative SWIPT NOMA is presented. In Section III, new analytical expressions are derived for the outage probability, diversity gain, and throughput when the proposed selection schemes, RNRF, NNNF, and NNFF, are used. Numerical results are presented in Section IV, which is followed by conclusion in Sections V.

II. Network Model

We consider a network with a single source S (i.e., the base station (BS)) and two groups of randomly deployed users $\{\mathrm{A_i}\}$ and $\{\mathrm{B_i}\}$. We assume that the users in group $\{\mathrm{B_i}\}$ are deployed within disc D_{B} with radius $R_{D_{\mathrm{B}}}$. The far users $\{\mathrm{A_i}\}$ are deployed within ring D_{A} with radius $R_{D_{\mathrm{C}}}$ and $R_{D_{\mathrm{A}}}$(assuming $R_{D_{\mathrm{C}}} \gg R_{D_{\mathrm{B}}}$), as shown in Fig. 1. Note that the BS is located at the origin of both the disc D_{B} and the ring D_{A}. The locations of the near and far users are modeled as homogeneous PPPs Φ_κ ($\kappa \in \{\mathrm{A}, \mathrm{B}\}$) with densities λ_{Φ_κ}. Here the near users are uniformly distributed within the disc and the far users are uniformly distributed within the ring. The number of users in R_{D_κ}, denoted by N_κ, follows a Poisson distribution $\Pr(N_\kappa = k) = (\mu_\kappa^k/k!)e^{-\mu_\kappa}$, where μ_κ is the mean measure, i.e., $\mu_{\mathrm{A}} = \pi\left(R_{D_{\mathrm{A}}}^2 - R_{D_{\mathrm{C}}}^2\right)\lambda_{\Phi_{\mathrm{A}}}$ and $\mu_{\mathrm{B}} = \pi R_{D_{\mathrm{B}}}^2 \lambda_{\Phi_{\mathrm{B}}}$. All channels are assumed to be quasi-static Rayleigh fading, where the channel coefficients are constant for each transmission block but vary independently between different blocks. In the proposed network, we consider that the users in $\{\mathrm{B_i}\}$ are energy harvesting relays that harvest energy from the BS and forward the information to $\{\mathrm{A_i}\}$ using the harvested energy as their transmit powers. The DF strategy is applied at $\{\mathrm{B_i}\}$ and the cooperative NOMA system consists of two phases, detailed in the following. In this work, without loss of generality, it is assumed that the two phases have the same transmission periods, the same as in [8, 10, 11]. It is worth pointing out that dynamic time allocation for the two phases may further improve the performance of the proposed cooperative NOMA scheme, but consideration of this issue is beyond the scope of the paper.

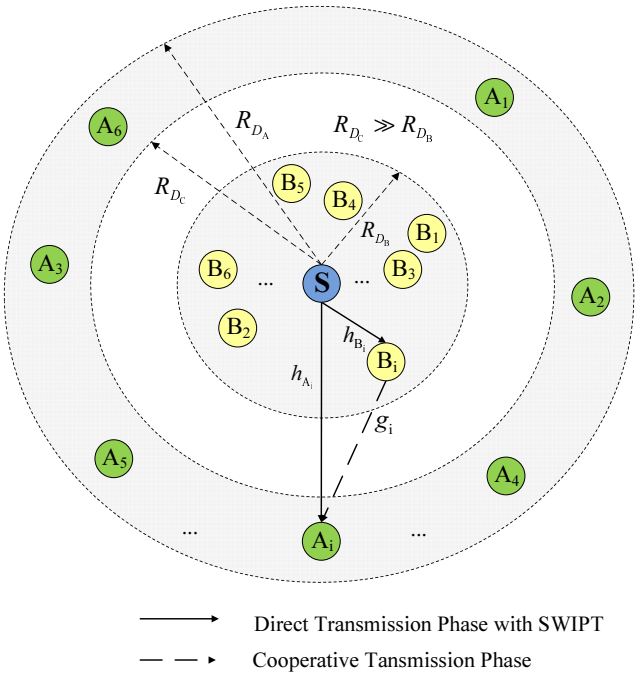

Fig. 1. An illustration of a aownlink SWIPT NOMA system with a base station S (blue circle). The spatial distributions of the near users (yellow circles) and the far users (green circles) follow homogeneous PPPs.

A. Phase 1: Direct Transmission

Prior to transmission, the two users denoted by $\mathrm{A_i}$ and $\mathrm{B_i}$, are selected to perform NOMA, where the selection criterion will be discussed in the next section. During the first phase, the BS sends two messages $p_{i1}x_{i1} + p_{i2}x_{i2}$ to two selected users $\mathrm{A_i}$ and $\mathrm{B_i}$ based on NOMA [3], where p_{i1} and p_{i2} are the power allocation coefficients and x_{i1} and x_{i2} are the messages of $\mathrm{A_i}$ and $\mathrm{B_i}$, respectively. The observation at $\mathrm{A_i}$ is given by

$$y_{\mathrm{A_i},1} = \sqrt{P_\mathrm{S}} \sum_{k\in\{1,2\}} p_{ik}x_{ik}\frac{h_{\mathrm{A_i}}}{\sqrt{1+d_{\mathrm{A_i}}^{\alpha}}} + n_{\mathrm{A_i},1}, \quad (1)$$

where P_S is the transmit power at the BS, $h_{\mathrm{A_i}}$ models the small-scale Rayleigh fading from the BS to $\mathrm{A_i}$ with $h_{\mathrm{A_i}} \sim \mathcal{CN}(0,1)$, $n_{\mathrm{A_i},1}$ is additive Gaussian white noise (AWGN) at $\mathrm{A_i}$ with variance $\sigma^2_{\mathrm{A_i}}$, $d_{\mathrm{A_i}}$ is the distance between BS and $\mathrm{A_i}$, and α is the path loss exponent.

Without loss of generality, we assume that $|p_{i1}|^2 > |p_{i2}|^2$ with $|p_{i1}|^2 + |p_{i2}|^2 = 1$. The received signal to interference and noise ratio (SINR) at $\mathrm{A_i}$ to detect x_{i1} is given by

$$\gamma_{\mathrm{S,A_i}}^{x_{i1}} = \frac{\rho|h_{\mathrm{A_i}}|^2|p_{i1}|^2}{\rho|p_{i2}|^2|h_{\mathrm{A_i}}|^2 + 1 + d_{\mathrm{A_i}}^{\alpha}}, \quad (2)$$

where $\rho = \frac{P_\mathrm{S}}{\sigma^2}$ is the transmit signal to noise radio (SNR) (assuming $\sigma^2_{\mathrm{A_i}} = \sigma^2_{\mathrm{B_i}} = \sigma^2$).

We consider that the near users have rechargeable storage ability [8] and power splitting [7] is applied to perform SWIPT. From the implementation point of view, this rechargeable storage unit can be a supercapacitor or a short-term high-efficiency battery [9]. The power splitting approach is applied as explained in the following: the observation at $\mathrm{B_i}$ is divided into two parts. One part is used for information decoding by directing the observation flow to the detection circuit and the remaining part is used for energy harvesting to powers $\mathrm{B_i}$ for helping $\mathrm{A_i}$. Thus,

$$y_{\mathrm{B_i},1} = \sqrt{P_\mathrm{S}} \sum_{k\in\{1,2\}} p_{ik}x_{ik}\frac{\sqrt{1-\beta_i}h_{\mathrm{B_i}}}{\sqrt{1+d_{\mathrm{B_i}}^{\alpha}}} + n_{\mathrm{B_i},1}, \quad (3)$$

where β_i is the power splitting coefficient which is detailed in (7), $h_{\mathrm{B_i}}$ models the small-scale Rayleigh fading from the BS to $\mathrm{B_i}$ with $h_{\mathrm{B_i}} \sim \mathcal{CN}(0,1)$, $n_{\mathrm{B_i}}$ is AWGN at $n_{\mathrm{B_i},1}$ with variance $\sigma^2_{\mathrm{B_i}}$, and $d_{\mathrm{B_i}}$ is the distance between the BS and $\mathrm{B_i}$. We use the bounded path loss model to ensure that the path loss is always larger than one even for small distances [10].

Applying NOMA, successive interference cancellation (SIC) [12] is carried out at $\mathrm{B_i}$. Particularly, $\mathrm{B_i}$ first decodes the message of $\mathrm{A_i}$, then subtracts this component from the received signal to detect its own information. Therefore, the received SINR at $\mathrm{B_i}$ to detect x_{i1} of $\mathrm{A_i}$ is given by

$$\gamma_{\mathrm{S,B_i}}^{x_{i1}} = \frac{\rho|h_{\mathrm{B_i}}|^2|p_{i1}|^2(1-\beta_i)}{\rho|h_{\mathrm{B_i}}|^2|p_{i2}|^2(1-\beta_i) + 1 + d_{\mathrm{B_i}}^{\alpha}}. \quad (4)$$

The received SNR at $\mathrm{B_i}$ to detect x_{i2} of $\mathrm{B_i}$ is given by

$$\gamma_{\mathrm{S,B_i}}^{x_{i2}} = \frac{\rho|h_{\mathrm{B_i}}|^2|p_{i2}|^2(1-\beta_i)}{1 + d_{\mathrm{B_i}}^{\alpha}}. \quad (5)$$

The power splitting coefficient β_i is used to determine the amount of harvested energy. Based on (4), the data rate supported by the channel from the BS to $\mathrm{B_i}$ for decoding x_{i1} is given by

$$R_{x_{i1}} = \frac{1}{2}\log\left(1 + \frac{\rho|h_{\mathrm{B_i}}|^2|p_{i1}|^2(1-\beta_i)}{\rho|h_{\mathrm{B_i}}|^2|p_{i2}|^2(1-\beta_i) + 1 + d_{\mathrm{B_i}}^{\alpha}}\right). \quad (6)$$

We assume that the energy required to receive/process information is negligible compared to the energy required for information transmission [8]. In this work, we apply the dynamic power splitting protocol which means that the power splitting coefficient β_i is a variable and opportunistically tuned to support the relay transmission. Our aim is to first guarantee the detection of the message of the far NOMA user, $\mathrm{A_i}$, at the near NOMA user $\mathrm{B_i}$, then $\mathrm{B_i}$ can harvest the remaining energy. In this case, based on (6), in order to ensure that $\mathrm{B_i}$ can successfully decode the information of $\mathrm{A_i}$, we have a rate, i.e., $R_1 = R_{x_{i1}}$. Therefore, the power splitting coefficient is set as follows:

$$\beta_i = \max\left\{0, 1 - \frac{\tau_1\left(1+d_{\mathrm{B_i}}^{\alpha}\right)}{\rho\left(|p_{i1}|^2 - \tau_1|p_{i2}|^2\right)|h_{\mathrm{B_i}}|^2}\right\}, \quad (7)$$

where $\tau_1 = 2^{2R_1} - 1$. Here $\beta_i = 0$ means that all the energy is used for information decoding and no energy remains for energy harvesting.

Based on (3), the energy harvested at $\mathrm{B_i}$ is given by

$$E_{\mathrm{B_i}} = \frac{T\eta P_\mathrm{S}\beta_i|h_{\mathrm{B_i}}|^2}{2\left(1+d_{\mathrm{B_i}}^{\alpha}\right)}, \quad (8)$$

where T is the time period for the entire transmission including the direct transmission phase and the cooperative transmission phase, and η is the energy harvesting coefficient. We assume

that the two phases have the same transmission period, and therefore, the transmit power at $\mathrm{B_i}$ can be expressed as follows:

$$P_t = \frac{\eta P_{\mathrm{S}} \beta_i |h_{\mathrm{B_i}}|^2}{1 + d_{\mathrm{B_i}}^{\alpha}}. \tag{9}$$

B. Phase 2: Cooperative Transmission

During this phase, $\mathrm{B_i}$ forwards x_{i1} to $\mathrm{A_i}$ by using the harvested energy during the direct transmission phase. In this case, $\mathrm{A_i}$ observes

$$y_{\mathrm{A_i},2} = \frac{\sqrt{P_t} x_{i1} g_{\mathrm{i}}}{\sqrt{1 + d_{\mathrm{C_i}}^{\alpha}}} + n_{\mathrm{A_i},2}, \tag{10}$$

where g_{i} models the small-scale Rayleigh fading from $\mathrm{B_i}$ to $\mathrm{A_i}$ with $g_{\mathrm{i}} \sim \mathcal{CN}(0,1)$, $n_{\mathrm{A_i},2}$ is AWGN at $\mathrm{A_i}$ with variance $\sigma^2_{\mathrm{A_i}}$, $d_{\mathrm{C_i}} = \sqrt{d^2_{\mathrm{A_i}} + d^2_{\mathrm{B_i}} - 2 d_{\mathrm{A_i}} d_{\mathrm{B_i}} \cos(\theta_i)}$ is the distance between $\mathrm{B_i}$ and $\mathrm{A_i}$, and θ_i denotes the angle $\angle \mathrm{A_i S B_i}$.

Based on (9) and (10), the received SNR for $\mathrm{A_i}$ to detect x_{i1} forwarded from $\mathrm{B_i}$ is given by

$$\gamma^{x_{i1}}_{\mathrm{A_i},\mathrm{B_i}} = \frac{P_t |g_i|^2}{\left(1 + d_{\mathrm{C_i}}^{\alpha}\right) \sigma^2} = \frac{\eta \rho \beta_i |h_{\mathrm{B_i}}|^2 |g_i|^2}{\left(1 + d_{\mathrm{C_i}}^{\alpha}\right)\left(1 + d_{\mathrm{B_i}}^{\alpha}\right)}. \tag{11}$$

At the end of this phase, $\mathrm{A_i}$ combines the signals from the BS and $\mathrm{B_i}$ using maximal-ratio combining (MRC). Combining the SNR of the direct transmission phase (2) and the SINR of the cooperative transmission phase (11), we obtain the received SINR at $\mathrm{A_i}$ as follows:

$$\gamma^{x_{i1}}_{\mathrm{A_i},\mathrm{MRC}} = \frac{\rho |h_{\mathrm{A_i}}|^2 |p_{i1}|^2}{\rho |h_{\mathrm{A_i}}|^2 |p_{i2}|^2 + 1 + d_{\mathrm{A_i}}^{\alpha}} + \frac{\eta \rho \beta_i |h_{\mathrm{B_i}}|^2 |g_i|^2}{\left(1 + d_{\mathrm{B_i}}^{\alpha}\right)\left(1 + d_{\mathrm{C_i}}^{\alpha}\right)}. \tag{12}$$

III. Non-Orthogonal Multiple Access with User Selection

In this section, the performance of three user selection schemes are characterized in the following.

A. RNRF Selection Scheme

In this scheme, the BS randomly selects a near user $\mathrm{B_i}$ and a far user $\mathrm{A_i}$. This selection scheme provides a fair opportunity for each user to access the source with the NOMA protocol. The advantage of this user selection scheme is that it does not require the knowledge of instantaneous channel state information (CSI). To make meaningful conclusions, in the rest of the paper, we only focus on $\beta_i > 0$ and the number of near users and far users satisfy $N_B \geq 1, N_A \geq 1$.

1) Outage Probability of the Near Users of RNRF: In the NOMA protocol, an outage of $\mathrm{B_i}$ can occur for two reasons. The first is that $\mathrm{B_i}$ cannot detect x_{i1}. The second is that $\mathrm{B_i}$ can detect x_{i1} but cannot detect x_{i2}. To guarantee that the NOMA protocol can be implemented, the condition $|p_{i1}|^2 - |p_{i2}|^2 \tau_1 > 0$ should be satisfied [3]. Based on this, the outage probability of $\mathrm{B_i}$ can be expressed as follows:

$$P_{\mathrm{B_i}} = \Pr\left(\frac{\rho |h_{\mathrm{B_i}}|^2 |p_{i1}|^2}{\rho |h_{\mathrm{B_i}}|^2 |p_{i2}|^2 + 1 + d_{\mathrm{B_i}}^{\alpha}} < \tau_1\right) + \Pr\left(\frac{\rho |h_{\mathrm{B_i}}|^2 |p_{i1}|^2}{\rho |h_{\mathrm{B_i}}|^2 |p_{i2}|^2 + 1 + d_{\mathrm{B_i}}^{\alpha}} > \tau_1, \gamma^{x_{i2}}_{\mathrm{S},\mathrm{B_i}} < \tau_2\right), \tag{13}$$

where $\tau_2 = 2^{2R_2} - 1$ with R_2 being the target rate at which $\mathrm{B_i}$ can detect x_{i2}.

The following theorem provides the outage probability of the near users in RNRF for an arbitrary choice of α.

Theorem 1: Conditioned on the PPPs, the outage probability of the near users $\mathrm{B_i}$ *can be approximated as follows:*

$$P_{\mathrm{B_i}} \approx \frac{1}{2} \sum_{n=1}^{N} \omega_N \sqrt{1 - \phi_n^2} \left(1 - e^{-c_n \varepsilon_{\mathrm{A}_i}}\right) (\phi_n + 1), \tag{14}$$

if $\varepsilon_{\mathrm{A}_i} \geq \varepsilon_{\mathrm{B}_i}$, *otherwise* $P_{\mathrm{B_i}} = 1$, *where* $\varepsilon_{\mathrm{A}_i} = \frac{\tau_1}{\rho\left(|p_{i1}|^2 - |p_{i2}|^2 \tau_1\right)}$ *and* $\varepsilon_{\mathrm{B}_i} = \frac{\tau_2}{\rho |p_{i2}|^2}$, N *is a parameter to ensure a complexity-accuracy tradeoff,* $c_n = 1 + \left(\frac{R_{D_{\mathrm{B}}}}{2}(\phi_n + 1)\right)^{\alpha}$, $\omega_N = \frac{\pi}{N}$, *and* $\phi_n = \cos\left(\frac{2n-1}{2N}\pi\right)$.

Proof: Define $X_i = \frac{|h_{\mathrm{A_i}}|^2}{1 + d^{\alpha}_{\mathrm{A_i}}}$, $Y_i = \frac{|h_{\mathrm{B_i}}|^2}{1 + d^{\alpha}_{\mathrm{B_i}}}$, and $Z_i = \frac{|g_i|^2}{1 + d^{\alpha}_{\mathrm{C_i}}}$. Substituting (4) and (5) into (13), the outage probability of the near users is given by

$$P_{\mathrm{B_i}} = \Pr\left(Y_i < \varepsilon_{\mathrm{A}_i}\right) + \Pr\left(Y_i > \varepsilon_{\mathrm{A}_i}, \varepsilon_{\mathrm{A}_i} < \varepsilon_{\mathrm{B}_i}\right). \tag{15}$$

If $\varepsilon_{\mathrm{A}_i} < \varepsilon_{\mathrm{B}_i}$, the outage probability at the near users is always one.

For the case $\varepsilon_{\mathrm{A}_i} \geq \varepsilon_{\mathrm{B}_i}$, note that the users are deployed in D_{B} and D_{A} according to homogeneous PPPs. Therefore, the NOMA users are modeled as independently and identically distributed (i.i.d.) points in D_{B} and D_{A}, denoted by W_{κ_i} ($\kappa \in \{\mathrm{A}, \mathrm{B}\}$), which contain the location information about $\mathrm{A_i}$ and $\mathrm{B_i}$, respectively. The probability density functions (PDFs) of $W_{\mathrm{A_i}}$ and $W_{\mathrm{B_i}}$ are given by

$$f_{W_{\mathrm{B_i}}}(\omega_{\mathrm{B_i}}) = \frac{\lambda_{\Phi_{\mathrm{B}}}}{\mu_{R_{D_{\mathrm{B}}}}} = \frac{1}{\pi R^2_{D_{\mathrm{B}}}}, \tag{16}$$

and

$$f_{W_{\mathrm{A_i}}}(\omega_{\mathrm{A_i}}) = \frac{\lambda_{\Phi_{\mathrm{A}}}}{\mu_{R_{D_{\mathrm{A}}}}} = \frac{1}{\pi\left(R^2_{D_{\mathrm{A}}} - R^2_{D_{\mathrm{C}}}\right)}, \tag{17}$$

respectively.

Therefore, for the case $\varepsilon_{\mathrm{A}_i} \geq \varepsilon_{\mathrm{B}_i}$, the cumulative distribution function (CDF) of Y_i is given by

$$\begin{aligned} F_{Y_i}(\varepsilon) &= \int_{D_{\mathrm{B}}} \left(1 - e^{-\left(1 + d^{\alpha}_{\mathrm{B_i}}\right)\varepsilon}\right) f_{W_{\mathrm{B_i}}}(\omega_{\mathrm{B_i}})\, d\omega_{\mathrm{B_i}} \\ &= \frac{2}{R^2_{D_{\mathrm{B}}}} \int_0^{R_{D_{\mathrm{B}}}} \left(1 - e^{-(1 + r^{\alpha})\varepsilon}\right) r dr. \end{aligned} \tag{18}$$

For many communication scenarios $\alpha > 2$, and it is challenging to obtain exact closed-from expressions for the above. In this case, we can use Gaussian-Chebyshev quadrature [13] to find the approximation of (18) as follows:

$$F_{Y_i}(\varepsilon) \approx \frac{1}{2} \sum_{n=1}^{N} \omega_N \sqrt{1 - \phi_n^2} \left(1 - e^{-c_n \varepsilon}\right) (\phi_n + 1). \tag{19}$$

Applying $\varepsilon_{\mathrm{A}_i} \to \varepsilon$ into (19), (14) is obtained, and the proof of the theorem is completed. ■

Corollary 1: For the special case $\alpha = 2$, *the outage probability of* $\mathrm{B_i}$ *can be obtained as follows:*

$$P_{\mathrm{B_i}}|_{\alpha=2} = 1 - \frac{e^{-\varepsilon_{\mathrm{A}_i}}}{R^2_{D_{\mathrm{B}}} \varepsilon_{\mathrm{A}_i}} + \frac{e^{-\left(1 + R^2_{D_{\mathrm{B}}}\right)\varepsilon_{\mathrm{A}_i}}}{R^2_{D_{\mathrm{B}}} \varepsilon_{\mathrm{A}_i}}, \tag{20}$$

if $\varepsilon_{\mathrm{A}_i} \geq \varepsilon_{\mathrm{B}_i}$, *otherwise* $P_{\mathrm{B_i}}|_{\alpha=2} = 1$.

Proof: Based on (18), when $\alpha = 2$ and after some manipulations, we can easily obtain

$$F_{Y_i}(\varepsilon)|_{\alpha=2} = 1 - \frac{e^{-\varepsilon}}{R_{D_\mathrm{B}}^2 \varepsilon} + \frac{e^{-\left(1+R_{D_\mathrm{B}}^2\right)\varepsilon}}{R_{D_\mathrm{B}}^2 \varepsilon}. \tag{21}$$

Applying $\varepsilon_{\mathrm{A}_i} \to \varepsilon$ into (21), (20) can be obtained. The proof is completed. ∎

2) Outage Probability of the Far Users of RNRF: With the proposed cooperative SWIPT NOMA protocol, outage experienced by $\mathrm{A_i}$ can occur in two situations. The first is when $\mathrm{B_i}$ can detect x_{i1} but the overall received SNR at $\mathrm{A_i}$ cannot support the targeted rate. The second is when neither $\mathrm{A_i}$ nor $\mathrm{B_i}$ can detect x_{i1}. Based on this, the outage probability can be expressed as follows:

$$\begin{aligned} P_{\mathrm{A_i}} =& \Pr\left(\gamma_{\mathrm{A_i,MRC}}^{x_{i1}} < \tau_1, \gamma_{\mathrm{S,B_i}}^{x_{i1}}\Big|_{\beta_i=0} > \tau_1\right) \\ &+ \Pr\left(\gamma_{\mathrm{S,A_i}}^{x_{i1}} < \tau_1, \gamma_{\mathrm{S,B_i}}^{x_{i1}}\Big|_{\beta_i=0} < \tau_1\right). \end{aligned} \tag{22}$$

The following theorem provides the outage probability of the far users in RNRF for an arbitrary choice of α.

Theorem 2: Conditioned on the PPPs, and assuming $R_{D_\mathrm{C}} \gg R_{D_\mathrm{B}}$, *the outage probability of* $\mathrm{A_i}$ *can be approximated as follows:*

$$\begin{aligned} P_{\mathrm{A_i}} \approx& \zeta_1 \sum_{n=1}^{N} (\phi_n + 1)\sqrt{1-{\phi_n}^2} c_n \sum_{k=1}^{K} \sqrt{1-\psi_k^2} s_k (1+s_k^\alpha)^2 \\ &\times \sum_{m=1}^{M} \sqrt{1-\varphi_m^2} e^{-(1+s_k^\alpha)t_m} \chi_{t_m}\left(\ln\frac{\chi_{t_m}(1+s_k^\alpha)}{\eta\rho} c_n + 2c_0\right) \\ &+ a_1 \sum_{n=1}^{N} \sqrt{1-{\phi_n}^2} c_n (\phi_n+1) \sum_{k=1}^{K} \sqrt{1-{\psi_k}^2}(1+s_k^\alpha) s_k, \end{aligned} \tag{23}$$

where M *and* K *are parameters to ensure a complexity-accuracy tradeoff,* $\zeta_1 = -\frac{\varepsilon_{\mathrm{A}_i} R_{D_{\mathrm{B_i}}} \omega_N \omega_K \omega_M}{8\left(R_{D_{\mathrm{A_i}}} + R_{D_{\mathrm{C_i}}}\right)\eta\rho}$, $\chi_{t_m} = \tau_1 - \frac{\rho t_m |p_{i1}|^2}{\rho t_m |p_{i2}|^2 + 1}$, $t_m = \frac{\varepsilon_{\mathrm{A}_i}}{2}(\varphi_m + 1)$, $\omega_M = \frac{\pi}{M}$, $\varphi_m = \cos\left(\frac{2m-1}{2M}\pi\right)$, $s_k = \frac{R_{D_\mathrm{A}} - R_{D_\mathrm{C}}}{2}(\psi_k + 1) + R_{D_\mathrm{C}}$, $\omega_K = \frac{\pi}{K}$, $\psi_k = \cos\left(\frac{2k-1}{2K}\pi\right)$, $c_0 = -\frac{\varphi(1)}{2} - \frac{\varphi(2)}{2}$, *and* $a_1 = \frac{\omega_K \omega_N \varepsilon_{\mathrm{A}_1}^2}{2\left(R_{D_\mathrm{A}} + R_{D_\mathrm{C}}\right)}$.

Proof: See Appendix A. ∎

Corollary 2: For the special case $\alpha = 2$, *the outage probability of* $\mathrm{A_i}$ *can be simplified as follows:*

$$\begin{aligned} P_{\mathrm{A_i}}|_{\alpha=2} \approx& \zeta_2 \sum_{k=1}^{K} \sqrt{1-\psi_k^2} s_k \left(1+s_k^2\right)^2 \sum_{m=1}^{M} \sqrt{1-\varphi_m^2} \\ &\times \chi_{t_m} e^{-\left(1+s_k^2\right)t_m}\left(\ln\frac{\chi_{t_m}\left(1+s_k^2\right)}{\eta\rho} c_n + b_0\right) \\ &+ \left(1 - \frac{e^{-\left(1+R_{D_\mathrm{C}}^2\right)\varepsilon_{\mathrm{A}_i}}}{\varepsilon_{\mathrm{A}_i}\left(R_{D_\mathrm{A}}^2 - R_{D_\mathrm{C}}^2\right)} + \frac{e^{-\left(1+R_{D_\mathrm{A}}^2\right)\varepsilon_{\mathrm{A}_i}}}{\varepsilon_{\mathrm{A}_i}\left(R_{D_\mathrm{A}}^2 - R_{D_\mathrm{C}}^2\right)}\right) \\ &\times \left(1 - \frac{e^{-\varepsilon_{\mathrm{A}_i}}}{R_{D_\mathrm{B}}^2 \varepsilon_{\mathrm{A}_i}} + \frac{e^{-\left(1+R_{D_\mathrm{B}}^2\right)\varepsilon_{\mathrm{A}_i}}}{R_{D_\mathrm{B}}^2 \varepsilon_{\mathrm{A}_i}}\right), \end{aligned} \tag{24}$$

where $\zeta_2 = -\frac{\omega_K \omega_M \varepsilon_{\mathrm{A}_i}\left(R_{D_\mathrm{B}}^2 + 2\right)}{8\left(R_{D_\mathrm{A}} + R_{D_\mathrm{C}}\right)\eta\rho}$ and $b_0 = \frac{\left(1+R_{D_\mathrm{B}}^2\right)^2 \ln\left(1+R_{D_\mathrm{B}}^2\right)}{2R_{D_\mathrm{B}}^2} + \left(R_{D_\mathrm{B}}^2 + 2\right)\left(c_0 - \frac{1}{4}\right)$.

Proof: See Appendix B. ∎

3) Diversity Analysis of RNRF: To obtain further insights into the derived outage probability, we provide a diversity analysis of both the near and far users of RNRF.

Near users: For the near users, based on the analytical results, we carry out high SNR approximations as follows. When $\varepsilon \to 0$, a high SNR approximation of (19) with $1 - e^{-x} \approx x$ is given by

$$F_{Y_i}(\varepsilon) \approx \frac{1}{2}\sum_{n=1}^{N} \omega_N \sqrt{1-{\phi_n}^2} c_n \varepsilon_{\mathrm{A}_i}(\phi_n + 1). \tag{25}$$

The diversity gain is defined as follows:

$$d = -\lim_{\rho\to\infty} \frac{\log P(\rho)}{\log\rho}. \tag{26}$$

Substituting (25) into (26), we obtain that the diversity gain for the near users is one, which means that using NOMA with energy harvesting will not decrease the diversity gain.

Far users: For the far users, substituting (23) into (26), we obtain

$$\begin{aligned} d =& -\lim_{\rho\to\infty} \frac{\log\left(-\frac{1}{\rho^2}\log\frac{1}{\rho}\right)}{\log\rho} \\ =& -\lim_{\rho\to\infty} \frac{\log\log\rho - \log\rho^2}{\log\rho} = 2. \end{aligned} \tag{27}$$

As we can see from (27), the diversity gain of RNRF is two, which is the same as that of the conventional cooperative network [14]. This result indicates that using NOMA with an energy harvesting relay will not affect the diversity gain. In addition, we see that at high SNRs, the dominant factor for the outage probability is $\frac{1}{\rho^2}\ln\rho$. Therefore we conclude that the outage probability of using NOMA with SWIPT decays at a rate of $\frac{\ln SNR}{SNR^2}$. However, for a conventional cooperative system without energy harvesting, a faster decreasing rate of $\frac{1}{SNR^2}$ can be achieved.

4) System Throughput in Delay-Sensitive Transmission Mode of RNRF: In this paper, we will focus on the delay-sensitive throughput. In this mode, the transmitter sends information at a fixed rate and the throughput is determined by evaluating the outage probability.

Based on the analytical results for the outage probability of the near and far users, the system throughput of RNRF in the delay-sensitive transmission mode is given by

$$R_{\tau_{\mathrm{RNRF}}} = (1 - P_{\mathrm{A_i}})R_1 + (1 - P_{\mathrm{B_i}})R_2, \tag{28}$$

where $P_{\mathrm{A_i}}$ and $P_{\mathrm{B_i}}$ are obtained from (23) and (14), respectively.

B. NNNF Selection Scheme

In this subsection, we characterize the performance of NNNF, which exploits the users' CSI opportunistically. We first select a user within the disc D_B which has the shortest distance to the BS as the near NOMA user (denoted by B_{i^*}).

This is because the near users also act as energy harvesting relays to help the far users. The NNNF scheme can enable the selected near user to harvest more energy. Then we select a user within the ring $D_{\rm A}$ which has the shortest distance to the BS as the far NOMA user (denoted by A_{i^*}). The advantage of the NNNF scheme is that it can minimize the outage probability of both the near and far users.

1) Outage Probability of the Near Users of NNNF: Using the same definition of the outage probability as the near users of NOMA, we can characterize the outage probability of the near users of NNNF.

The following theorem provides the outage probability of the near users of NNNF for an arbitrary choice of α.

Theorem 3: Conditioned on the PPPs, the outage probability of B_{i^*} *can be approximated as follows:*

$$P_{\mathrm{B}_{i^*}} \approx b_1 \sum_{n=1}^{N} \sqrt{1-{\phi_n}^2}\left(1-e^{-(1+c_{n*}^{\alpha})\varepsilon_{\mathrm{A}_i}}\right) c_{n*} e^{-\pi\lambda_{\Phi_{\mathrm{B}}} c_{n*}^2}, \tag{29}$$

if $\varepsilon_{\mathrm{A}_i} \geq \varepsilon_{\mathrm{B}_i}$, *otherwise* $P_{\mathrm{B}_{i^*}} = 1$, *where* $c_{n*} = \frac{R_{D_{\mathrm{B}}}}{2}(\phi_n+1)$, $b_1 = \frac{\xi_{\mathrm{B}}\omega_N R_{D_{\mathrm{B}}}}{2}$, *and* $\xi_{\mathrm{B}} = \frac{2\pi\lambda_{\Phi_{\mathrm{B}}}}{1-e^{-\pi\lambda_{\Phi_{\mathrm{B}}}R_{D_{\mathrm{B}}}^2}}$.

Proof: Similar to (15), the outage probability of B_{i^*} can be expressed as follows:

$$P_{\mathrm{B}_{i^*}} = \Pr\left(Y_{i^*} < \varepsilon_{\mathrm{A}_i} \middle| N_{\mathrm{B}} \geq 1\right) = F_{Y_{i^*}}\left(\varepsilon_{\mathrm{A}_i}\right), \tag{30}$$

where $Y_{i^*} = \frac{|h_{\mathrm{B}_i}|^2}{1+d_{\mathrm{B}_{i^*}}^{\alpha}}$ and $d_{\mathrm{B}_{i^*}}$ is the distance from the nearest B_{i^*} to the BS.

The CDF of Y_{i^*} can be written as follows:

$$F_{Y_{i^*}}(\varepsilon) = \int_0^{R_{D_{\mathrm{B}}}} \left(1-e^{-(1+r_{\mathrm{B}}^{\alpha})\varepsilon}\right) f_{d_{\mathrm{B}_{i^*}}}(r_{\mathrm{B}})\, dr_{\mathrm{B}}, \tag{31}$$

where $f_{d_{\mathrm{B}_{i^*}}}$ is the PDF of the shortest distance from B_{i^*} to the BS.

The probability $\Pr\{d_{\mathrm{B}_{i^*}} > r | N_{\mathrm{B}} \geq 1\}$ conditioned on $N_{\mathrm{B}} \geq 1$ is the event that there is no point located in the disc. Therefore we can express this probability as follows:

$$\begin{aligned}
&\Pr\{d_{\mathrm{B}_{i^*}} > r | N_{\mathrm{B}} \geq 1\} \\
=&\frac{\Pr\{d_{\mathrm{B}_{i^*}} > r\} - \Pr\{d_{\mathrm{B}_{i^*}} > r, N_{\mathrm{B}} = 0\}}{\Pr\{N_{\mathrm{B}} \geq 1\}} \\
=&\frac{e^{-\pi\lambda_{\Phi_{\mathrm{B}}} r^2} - e^{-\pi\lambda_{\Phi_{\mathrm{B}}} R_{D_{\mathrm{B}}}^2}}{1-e^{-\pi\lambda_{\Phi_{\mathrm{B}}} R_{D_{\mathrm{B}}}^2}}.
\end{aligned} \tag{32}$$

Then the corresponding PDF of B_{i^*} is given by

$$f_{d_{\mathrm{B}_{i^*}}}(r_{\mathrm{B}}) = \xi_{\mathrm{B}} r_{\mathrm{B}} e^{-\pi\lambda_{\Phi_{\mathrm{B}}} r_{\mathrm{B}}^2}. \tag{33}$$

Substituting (33) into (31), we obtain

$$F_{Y_{i^*}}(\varepsilon) = \xi_{\mathrm{B}} \int_0^{R_{D_{\mathrm{B}}}} \left(1-e^{-(1+r_{\mathrm{B}}^{\alpha})\varepsilon}\right) r_{\mathrm{B}} e^{-\pi\lambda_{\Phi_{\mathrm{B}}} r_{\mathrm{B}}^2} dr_{\mathrm{B}}. \tag{34}$$

Applying the Gaussian-Chebyshev quadrature approximation to (19), we obtain

$$\begin{aligned}
F_{Y_{i^*}}(\varepsilon) \approx& \frac{\xi_{\mathrm{B}}\omega_N R_{D_{\mathrm{B}}}}{2} \\
&\times \sum_{n=1}^{N} \sqrt{1-{\phi_n}^2}\left(1-e^{-(1+c_{n*}^{\alpha})\varepsilon}\right) c_{n*} e^{-\pi\lambda_{\Phi_{\mathrm{B}}} c_{n*}^2}.
\end{aligned} \tag{35}$$

Applying $\varepsilon_{\mathrm{A}_i} \to \varepsilon$, we obtain the approximate outage probability of B_{i^*} in (29). ■

Based on (34) and after some manipulations, the following corollary can be obtained.

Corollary 3: For the special case $\alpha = 2$, *the outage probability of* B_{i^*} *can be expressed as follows:*

$$\begin{aligned}
P_{\mathrm{B}_{i^*}}|_{\alpha=2} =& \frac{\xi_{\mathrm{B}}\left(e^{-R_{D_{\mathrm{B}}}^2\left(\pi\lambda_{\Phi_{\mathrm{B}}}+\varepsilon_{\mathrm{A}_i}\right)-\varepsilon_{\mathrm{A}_i}} - e^{-\varepsilon_{\mathrm{A}_i}}\right)}{2\left(\pi\lambda_{\Phi_{\mathrm{B}}}+\varepsilon_{\mathrm{A}_i}\right)} \\
&- \frac{\xi_{\mathrm{B}}\left(e^{-\pi\lambda_{\Phi_{\mathrm{B}}}R_{D_{\mathrm{B}}}^2}-1\right)}{2\pi\lambda_{\Phi_{\mathrm{B}}}},
\end{aligned} \tag{36}$$

if $\varepsilon_{\mathrm{A}_i} \geq \varepsilon_{\mathrm{B}_i}$, *otherwise* $P_{\mathrm{B}_{i^*}}|_{\alpha=2} = 1$.

2) Outage Probability of the Far Users of NNNF: Using the same definition of the outage probability for the far users of NOMA, and similar to (22), we can characterize the outage probability of the far users in NNNF. The following theorem provides the outage probability of the far users in NNNF for an arbitrary choice of α.

Theorem 4: Conditioned on the PPPs and assuming $R_{D_{\mathrm{C}}} \gg R_{D_{\mathrm{B}}}$, *the outage probability of* A_{i^*} *can be approximated as follows:*

$$\begin{aligned}
P_{\mathrm{A}_{i^*}} \approx& \varsigma^* \sum_{n=1}^{N} \sqrt{1-{\phi_n}^2}\left(1+c_{n*}^{\alpha}\right) c_{n*} e^{-\pi\lambda_{\Phi_{\mathrm{B}}} c_{n*}^2} \\
&\times \sum_{k=1}^{K} \sqrt{1-\psi_k^2}(1+s_k^{\alpha})^2 s_k e^{-\pi\lambda_{\Phi_{\mathrm{A}}}\left(s_k^2-R_{D_{\mathrm{C}}}^2\right)} \sum_{m=1}^{M} \sqrt{1-\varphi_m^2} \\
&\times e^{-(1+s_k^{\alpha})t_m} \chi_{t_m}\left(\ln\frac{\chi_{t_m}\left(1+s_k^{\alpha}\right)\left(1+c_{n*}^{\alpha}\right)}{\eta\rho} + 2c_0\right) \\
&+ b_2 b_3 \sum_{k=1}^{K} \sqrt{1-{\psi_k}^2}(1+s_k^{\alpha}) s_k e^{-\pi\lambda_{\Phi_{\mathrm{A}}} s_k^2} \\
&\times \sum_{n=1}^{N}\left(\sqrt{1-{\phi_n}^2}\left(1+c_{n*}^{\alpha}\right) c_{n*} e^{-\pi\lambda_{\Phi_{\mathrm{B}}} c_{n*}^2}\right),
\end{aligned} \tag{37}$$

where $\varsigma^* = -\frac{\xi_{\mathrm{B}}\xi_{\mathrm{A}}\omega_N\omega_K\omega_M\varepsilon_{\mathrm{A}_i}R_{D_{\mathrm{B}}}\left(R_{D_{\mathrm{A}}}-R_{D_{\mathrm{C}}}\right)}{8\eta\rho}$, $b_2 = \frac{\xi_{\mathrm{A}} e^{\pi\lambda_{\Phi_{\mathrm{A}}} R_{D_{\mathrm{C}}}^2}\omega_K\varepsilon_{\mathrm{A}_i}}{R_{D_{\mathrm{A}}}+R_{D_{\mathrm{C}}}}$, *and* $b_3 = \frac{\xi_{\mathrm{B}}\omega_N R_{D_{\mathrm{B}}}\varepsilon_{\mathrm{A}_i}}{2}$.

Proof: See Appendix C. ■

Corollary 4: For the special case $\alpha = 2$, *the outage probability of* A_{i^*} *can be simplified as* (38) *at the top of the following page.*

Proof: For the special case $\alpha = 2$, after some manipulations, we can express (C.11) as follows:

$$\begin{aligned}
F_{X_{i^*}}(\varepsilon)|_{\alpha=2} =& -\frac{\xi_{\mathrm{A}}\left(e^{\pi\lambda_{\Phi_{\mathrm{A}}}\left(R_{D_{\mathrm{C}}}^2-R_{D_{\mathrm{A}}}^2\right)}-1\right)}{2\pi\lambda_{\Phi_{\mathrm{A}}}} \\
&+ \frac{\xi_{\mathrm{A}} e^{\pi\lambda_{\Phi_{\mathrm{A}}}R_{D_{\mathrm{C}}}^2} e^{-\varepsilon}}{2\left(\pi\lambda_{\Phi_{\mathrm{A}}}+\varepsilon\right)}\left(e^{-R_{D_{\mathrm{A}}}^2\left(\pi\lambda_{\Phi_{\mathrm{A}}}+\varepsilon\right)} - e^{-R_{D_{\mathrm{C}}}^2\left(\pi\lambda_{\Phi_{\mathrm{A}}}+\varepsilon\right)}\right).
\end{aligned} \tag{39}$$

Based on (C.10), combining (39) and (36), and setting $\alpha = 2$ into (C.9), we can obtain (38). The proof is completed. ■

$$P_{\mathrm{A}_{i^*}}|_{\alpha=2} \approx \varsigma^* \sum_{n=1}^{N} \sqrt{1-\phi_n{}^2}\left(1+c_{n*}^2\right) c_{n*} e^{-\pi\lambda_{\Phi_\mathrm{B}} c_{n*}^2} \sum_{k=1}^{K} \sqrt{1-\psi_k^2}\left(1+s_k^2\right)^2 s_k e^{-\pi\lambda_{\Phi_\mathrm{A}}\left(s_k^2-R_{D_\mathrm{C}}^2\right)}$$
$$\times \sum_{m=1}^{M} \sqrt{1-\varphi_m^2}\left(e^{-\left(1+s_k^2\right)t_m}\chi_{t_m}\left(\ln\frac{\chi_{t_m}\left(1+s_k^2\right)\left(1+c_{n*}^2\right)}{\eta\rho}+2c_0\right)\right)$$
$$+\frac{\xi_\mathrm{A} e^{\pi\lambda_{\Phi_\mathrm{A}} R_{D_\mathrm{C}}^2}}{2}\left(\frac{e^{-\varepsilon_{\mathrm{A}_i}}}{\pi\lambda_{\Phi_\mathrm{A}}+\varepsilon_{\mathrm{A}_i}}\left(e^{-R_{D_\mathrm{A}}^2\left(\pi\lambda_{\Phi_\mathrm{A}}+\varepsilon_{\mathrm{A}_i}\right)}-e^{-R_{D_\mathrm{C}}^2\left(\pi\lambda_{\Phi_\mathrm{A}}+\varepsilon_{\mathrm{A}_i}\right)}\right)-\frac{\left(e^{-\pi\lambda_{\Phi_\mathrm{A}} R_{D_\mathrm{A}}^2}-e^{-\pi\lambda_{\Phi_\mathrm{A}} R_{D_\mathrm{C}}^2}\right)}{\pi\lambda_{\Phi_\mathrm{A}}}\right)$$
$$\times \frac{\xi_\mathrm{B}}{2}\left(\frac{e^{-R_{D_\mathrm{B}}^2\left(\pi\lambda_{\Phi_\mathrm{B}}+\varepsilon_{\mathrm{A}_i}\right)-\varepsilon_{\mathrm{A}_i}}-e^{-\varepsilon_{\mathrm{A}_i}}}{\pi\lambda_{\Phi_\mathrm{B}}+\varepsilon_{\mathrm{A}_i}}-\frac{e^{-\pi\lambda_{\Phi_\mathrm{B}} R_{D_\mathrm{B}}^2}-1}{\pi\lambda_{\Phi_\mathrm{B}}}\right). \tag{38}$$

3) Diversity Analysis of NNNF: Similarly, we provide diversity analysis of both the near and far users of NNNF.

Near users: For the near users, based on the analytical results, we carry out the high SNR approximation as follows. When $\varepsilon \to 0$, a high SNR approximation of (29) with $1-e^{-x}\approx x$ is given by

$$P_{\mathrm{B}_{i^*}} \approx b_1 \varepsilon_{\mathrm{A}_i} \sum_{n=1}^{N}\left(\sqrt{1-\phi_n{}^2}\left(1+c_{n*}^{\alpha}\right) c_{n*} e^{-\pi\lambda_{\Phi_\mathrm{B}} c_{n*}^2}\right). \tag{40}$$

Substituting (40) into (26), we obtain that the diversity gain for the near users of NNNF is one, which indicates that using NNNF will not affect the diversity gain.

Far users: For the far users, substituting (37) into (26), we obtain that the diversity gain is still two. This indicates that NNNF will not affect the diversity gain.

4) System Throughput in Delay-Sensitive Transmission Mode of NNNF: Based on the analytical results for the outage probability of the near and far users, the system throughput of NNNF in the delay-sensitive transmission mode is given by

$$R_{\tau_{\mathrm{NNNF}}} = \left(1-P_{\mathrm{A}_{i^*}}\right) R_1 + \left(1-P_{\mathrm{B}_{i^*}}\right) R_2, \tag{41}$$

where $P_{\mathrm{A}_{i^*}}$ and $P_{\mathrm{B}_{i^*}}$ are obtained from (37) and (29), respectively.

C. NNFF Selection Scheme

In this scheme, we first select a user within disc D_B which has the shortest distance to the BS as a near NOMA user. Then we select a user within ring D_A which has the farthest distance to the BS as a far NOMA user (denoted by $\mathrm{A}_{i'}$). The use of this selection scheme is inspired by an interesting observation described in [3] that NOMA can offer a larger performance gain over conventional MA when user channel conditions are more distinct.

1) Outage Probability of the Near Users of NNFF: Since the same criterion for the near users is used, the outage probabilities of near nears for an arbitrary α and the special case $\alpha=2$ are the same as those expressed in (29) and (36), respectively.

2) Outage Probability of the Far Users of NNFF: Using the same definition of the outage probability of the far users, and similar to (22), we can characterize the outage probability of the far users of NNFF. The following theorem provides the outage probability of the far user of NNFF for an arbitrary choice of α.

Theorem 5: Conditioned on the PPPs and assuming $R_{D_\mathrm{C}} \gg R_{D_\mathrm{B}}$, the outage probability of $\mathrm{A}_{i'}$ can be approximated as follows:

$$P_{\mathrm{A}_{i'}} \approx \varsigma^* \sum_{n=1}^{N} \sqrt{1-\phi_n{}^2}\left(1+c_{n*}^{\alpha}\right) c_{n*} e^{-\pi\lambda_{\Phi_\mathrm{B}} c_{n*}^2}$$
$$\times \sum_{k=1}^{K} \sqrt{1-\psi_k^2}\left(1+s_k^{\alpha}\right)^2 s_k e^{-\pi\lambda_{\Phi_\mathrm{A}}\left(R_{D_\mathrm{A}}^2-s_k^2\right)} \sum_{m=1}^{M} \sqrt{1-\varphi_m^2}$$
$$\times e^{-\left(1+s_k^{\alpha}\right)t_m}\chi_{t_m}\left(\ln\frac{\chi_{t_m}\left(1+s_k^{\alpha}\right)\left(1+c_{n*}^{\alpha}\right)}{\eta\rho}+2c_0\right)$$
$$+ b_3 b_4 \sum_{k=1}^{K} \sqrt{1-\psi_k{}^2}\left(1+s_k^{\alpha}\right) s_k e^{\pi\lambda_{\Phi_\mathrm{A}} s_k^2}$$
$$\times \sum_{n=1}^{N}\left(\sqrt{1-\phi_n{}^2}\left(1+c_{n*}^{\alpha}\right) c_{n*} e^{-\pi\lambda_{\Phi_\mathrm{B}} c_{n*}^2}\right), \tag{42}$$

where $b_4 = \frac{\xi_\mathrm{A} e^{-\pi\lambda_{\Phi_\mathrm{A}} R_{D_\mathrm{A}}^2}\omega_K \varepsilon_{\mathrm{A}_i}}{R_{D_\mathrm{A}}+R_{D_\mathrm{C}}}$.

Proof: See Appendix D. ∎

Corollary 5: For the special case $\alpha = 2$, after some manipulations, the outage probability of $\mathrm{A}_{i'}$ can be simplified as (43) *at the top of the next page.*

3) Diversity Analysis: Similarly, we provide diversity analysis of both the near and far uses in NNFF.

Near users: Since the same criterion for selecting a near user is used, the diversity gain is one, which is the same as for NNNF.

Far users: Substituting (42) into (26), we find that the diversity gain is still two. Therefore, we conclude that using opportunistic user selection schemes (NNNF and NNFF) based on distances will not affect the diversity gain.

4) System Throughput in Delay-Sensitive Transmission Mode of NNFF: Based on the analytical results for the outage probability of the near and far users, the system throughput of NNFF in the delay-sensitive transmission mode is given by

$$R_{\tau_{\mathrm{NNFF}}} = \left(1-P_{\mathrm{A}_{i'}}\right) R_1 + \left(1-P_{\mathrm{B}_{i^*}}\right) R_2, \tag{44}$$

$$P_{\mathrm{A}_{i'}}\big|_{\alpha=2} \approx \varsigma^* \sum_{n=1}^{N} \sqrt{1-\phi_n{}^2}\left(1+c_{n*}^2\right) c_{n*} e^{-\pi\lambda_{\Phi_\mathrm{B}} c_{n*}^2} \sum_{k=1}^{K} \sqrt{1-\psi_k^2}\left(1+s_k^2\right)^2 s_k e^{-\pi\lambda_{\Phi_\mathrm{A}}\left(R_{D_\mathrm{A}}^2 - s_k^2\right)}$$
$$\times \sum_{m=1}^{M} \sqrt{1-\varphi_m^2}\left(e^{-\left(1+s_k^2\right)t_m}\chi_{t_m}\left(\ln\frac{\chi_{t_m}\left(1+s_k^2\right)\left(1+c_{n*}^2\right)}{\eta\rho}+2c_0\right)\right)$$
$$+\frac{\xi_\mathrm{A} e^{-\pi\lambda_{\Phi_\mathrm{A}} R_{D_\mathrm{A}}^2}}{2}\left(\frac{e^{\pi\lambda_{\Phi_\mathrm{A}} R_{D_\mathrm{A}}^2} - e^{\pi\lambda_{\Phi_\mathrm{A}} R_{D_\mathrm{C}}^2}}{\pi\lambda_{\Phi_\mathrm{A}}} - \frac{e^{-\varepsilon_{\mathrm{A}_i}}}{\pi\lambda_{\Phi_\mathrm{A}}-\varepsilon_{\mathrm{A}_i}}\left(e^{R_{D_\mathrm{A}}^2\left(\pi\lambda_{\Phi_\mathrm{A}}-\varepsilon_{\mathrm{A}_i}\right)} - e^{R_{D_\mathrm{C}}^2\left(\pi\lambda_{\Phi_\mathrm{A}}-\varepsilon_{\mathrm{A}_i}\right)}\right)\right)$$
$$\times \frac{\xi_\mathrm{B}}{2}\left(\frac{\left(e^{-R_{D_\mathrm{B}}^2\left(\pi\lambda_{\Phi_\mathrm{B}}+\varepsilon_{\mathrm{A}_i}\right)-\varepsilon_{\mathrm{A}_i}} - e^{-\varepsilon_{\mathrm{A}_i}}\right)}{\left(\pi\lambda_{\Phi_\mathrm{B}}+\varepsilon_{\mathrm{A}_i}\right)} - \frac{\left(e^{-\pi\lambda_{\Phi_\mathrm{B}} R_{D_\mathrm{B}}^2}-1\right)}{\pi\lambda_{\Phi_\mathrm{B}}}\right). \tag{43}$$

where $P_{\mathrm{A}_{i'}}$ and $P_{\mathrm{B}_{i^*}}$ are obtained from (42) and (29), respectively.

IV. Numerical Results

In this section, numerical results are presented to facilitate the performance evaluations (including the outage probability of the near and the far users and the delay sensitive throughput) of the proposed cooperative SWIPT NOMA protocol. In the considered network, we assume that the energy conversion efficiency of SWIPT is $\eta = 0.7$ and the power allocation coefficients of NOMA is $|p_{i1}|^2 = 0.8$, $|p_{i1}|^2 = 0.2$. In the following figures, we use red, blue and black color lines to represent the RNRF, NNNF and NNFF user selection schemes, respectively.

A. Outage Probability of the Near Users

In this subsection, the outage probability achieved by the near users with different choices of density and path loss coefficients for the three user selection schemes is demonstrated. Note that the same user selection criterion is applied for the near users of NNNF and NNFF, we use NNN(F)F to represent these two selection schemes in Fig. 2, Fig. 3, and Fig. 4.

Fig. 2 plots the outage probability of the near users versus SNR with different path loss coefficients for both RNRF and NNN(F)F. The solid red and blue curves are for the special case $\alpha = 2$ of RNRF and NNN(F)F, corresponding to the analytical results derived in (20) and (36), respectively. The dashed red and blue curves are for an arbitrary choice of α, corresponding to the analytical results derived in (14) and (29), respectively. Monte Carlo simulation results are marked as "•" to verify our derivation. The figure shows precise agreement between the simulation and analytical curves. One can observe that by performing NNNF and NNFF (which we refer to as NNN(F)F in the figure), lower outage probability is achieved than with RNRF since shorter distances mean lower path loss and leads to better performance. The figure also demonstrates that as α increases, outage will occur more frequently because of higher path loss. For NNNF and NNFF, the performance is very close for different values of α. This is because we use the bounded path loss model (i.e. $1 + d_\mathrm{i}^\alpha > 1$) to ensure that the path loss is always larger than one. When selecting the nearest near user, d_i will approach zero and the path loss will approach one, which makes the performance difference of the three selection schemes insignificant. It is worth noting that all curves have the same slopes, which indicates that the diversity gains of the schemes are the same. This phenomenon validates the insights we obtained from the analytical results derived in (26). Fig. 2 also shows that if the choices of rates for users are incorrect (i.e., $R_1 = 0.5$ and $R_2 = 1$ in this figure), the outage probability of the near users will be always one, which verifies the analytical results in (14) and (29).

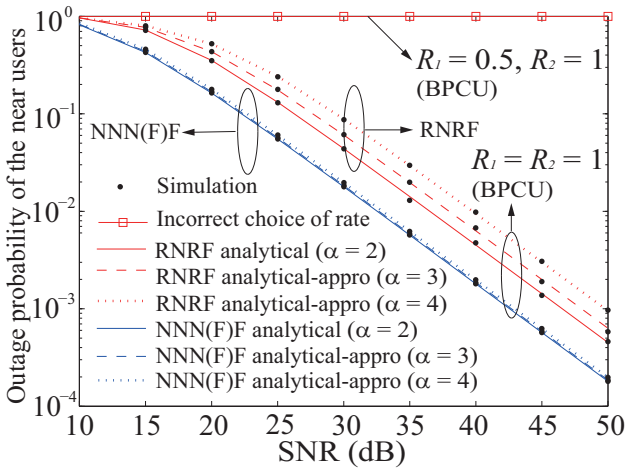

Fig. 2. Outage probability of the near users versus SNR with different α, where $R_{D_\mathrm{B}} = 2$ m, and $\lambda_{\Phi_\mathrm{B}} = 1$.

Fig. 3 plots the outage probability of the near users versus their density with different values of R_{D_B}. RNRF is also shown in the figure as a benchmark for comparison. Several observations are drawn as follows: 1) The outage probabilities of RNRF and NNN(F)F decrease with decreasing R_{D_B} because path loss is reduced; 2) The outage probability of NNN(F)F decreases as the density of the near users increases. This is due to the multiuser diversity gain, since there is an increasing number of the near users; 3) The outage probability of RNRF is a constant, i.e., independent of the density of near users, and is the outage ceiling of the NNN(F)F. This is due to the fact that no opportunistic user selection is carried out for RNRF; and 4) An outage floor exits even if the density of the near users goes to infinity. This is due to the bounded

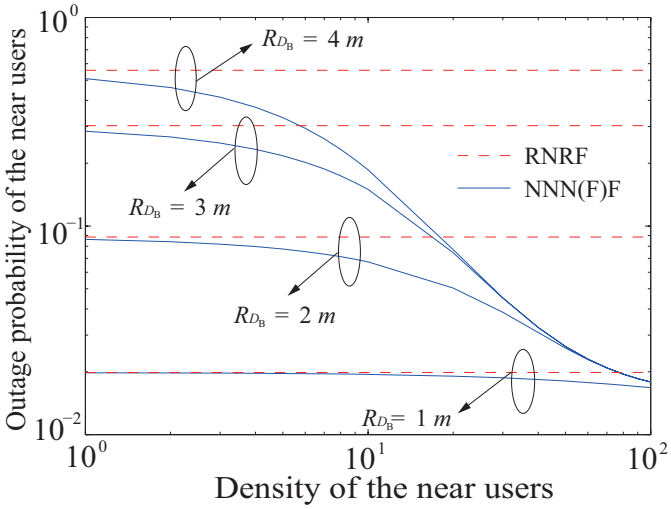

Fig. 3. Outage probability of the near users versus density with different R_{D_B}, where $\lambda_{\Phi_B} = 1$, and $SNR = 30$ dB.

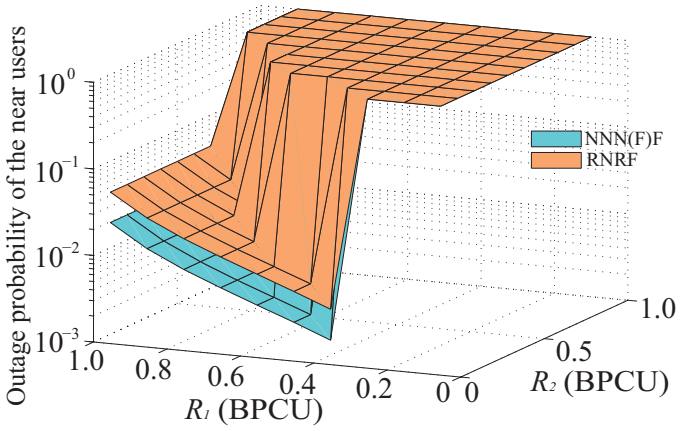

Fig. 4. Outage probability of the near users versus R_1 and R_2, where $\alpha = 2, R_{D_B} = 2$ m, and $SNR = 30$ dB.

path loss model we have used. When the number of the near users exceeds a threshold, the selected near user will be very close to the source, which makes the path gain approach one.

Fig. 4 plots the outage probability of the near users versus the rate of the near users and far users for both RNRF and NNN(F)F. One can observe that the outage of the near users occurs more frequently as the rate of the far user, R_1, increases. This is because in our proposed protocol, the near user $\mathrm{B_i}$ needs to first decode x_{i1} which is intended to the far user $\mathrm{A_i}$, and then decode its own message. Therefore increasing R_1 makes it harder to decode x_{i1}, which will lead to increased outages. An important observation is that incorrect choices of R_1 and R_2 will make the outage probability always one. Particularly, for the choice of R_1, it should satisfy the condition $(|p_{i1}|^2 - |p_{i2}|^2\tau_1 > 0)$ in order to ensure that successive interference cancelation can be implemented. For the choice of R_2, it should satisfy the condition that the split energy for detecting x_{i1} is also sufficient to detect x_{i2} $(\varepsilon_{\mathrm{A}_i} \geq \varepsilon_{\mathrm{B}_i})$.

B. Outage Probability of the Far Users

In this subsection, we demonstrate the outage probability of the far users with different choices of the density, path loss coefficients, and user zone of the three user selection schemes.

Fig. 5 plots the outage probability of the far users versus SNR with different path loss coefficients of RNRF, NNNF, and NNFF. The dashed red, blue, and black curves circled together and pointed by $\alpha = 2$, are the analytical approximations for the special case of RNRF, NNNF, and NNFF, which are obtained from (24), (38) and (43), respectively. The dashed red, blue, and black curves circled together and pointed by $\alpha = 3$, are the analytical approximations for an arbitrary choice of α of RNRF, NNNF, and NNFF, which are obtained from (23), (37) and (42), respectively. We use the solid marked lines to represent the Monte Carlo simulation results for each case. As can be observed from the figure, the simulation

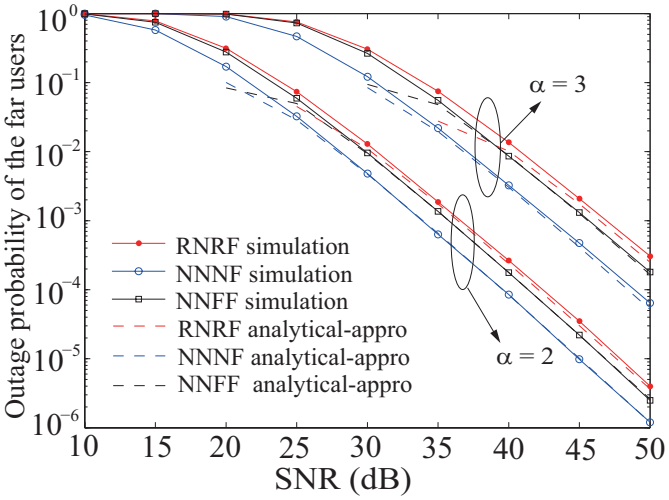

Fig. 5. Outage probability of the far users with different α, $R_1 = 0.3$ BPCU, $R_{D_A} = 10$ m, $R_{D_B} = 2$ m, $R_{D_C} = 8$ m, $\lambda_{\Phi_A} = 1$, and $\lambda_{\Phi_B} = 1$.

and the analytical approximation are very close, particularly in the high SNR region. Several observations can be drawn as follows: 1) NNNF achieves the lowest outage probability among the three selection schemes since both the near and far users have the smallest path loss; 2) NNFF achieves lower outage than RNRF, which indicates that the distance of the near users has more impact than that of the far users; 3) it is clear that all of the curves in Fig. 5 have the same slopes, which indicates that the diversity gains of the far users for the three schemes are the same. In the diversity analysis, we showed that the diversity gain of the three selection schemes is two. The simulation validates the analytical results and indicates that the achievable diversity gain is the same for different user selection schemes.

Fig. 6 plots the outage probability of the far users versus R_1 with different R_{D_C} and R_{D_B}. One can observe that the outage probabilities of the three schemes increase as R_1 increases. This is because increasing R_1 will make the threshold of

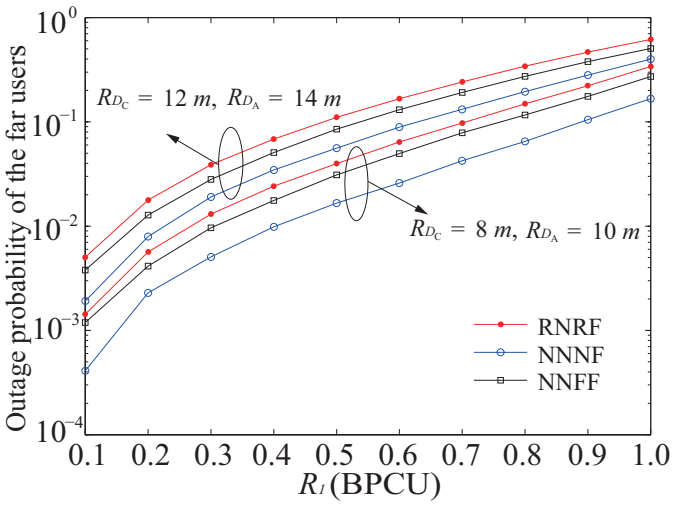

Fig. 6. Outage probability of the far users versus R_1, where $\alpha = 2$, $R_{D_B} = 2\ m$, and $SNR = 30$ dB.

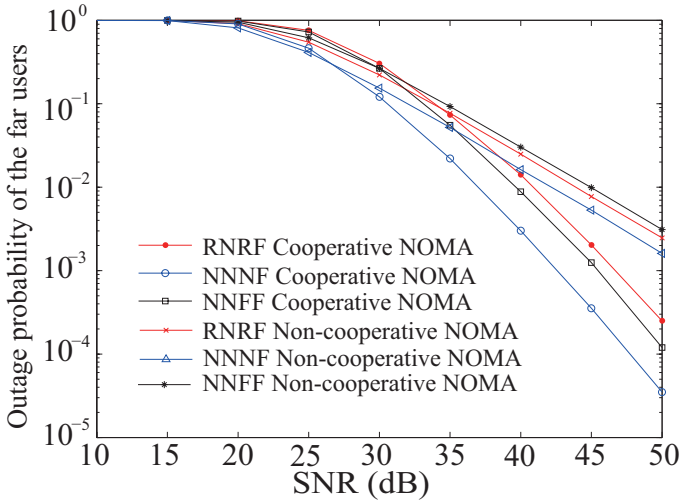

Fig. 7. Comparison of outage probability with non-cooperative NOMA, $\alpha = 3$, $R_1 = 0.3$ BPCU, $R_{D_A} = 10\ m$, $R_{D_B} = 2\ m$, $R_{D_C} = 8\ m$, $\lambda_{\Phi_A} = 1$, and $\lambda_{\Phi_B} = 1$.

decoding higher, which in turn leads to more outage. It can also be observed that increasing the radius of the user zone for the far users will deteriorate the outage performance. The reason is that the path loss of the far users becomes larger.

Fig. 7 plots the outage probability of the far users versus SNR for both cooperative NOMA and non-cooperative NOMA[1]. Several observations can be drawn as follows: 1) by using an energy constrained relay to perform cooperative NOMA transmission, the outage probability of the far users has a larger slope than that of non-cooperative NOMA, for all user selection schemes. This is due to the fact that cooperative NOMA can achieve a larger diversity gain and guarantees more reliable reception for the far users in the high SINR region; 2) NNNF achieves the lowest outage probability among these three selection schemes both for cooperative NOMA and non-cooperative NOMA because of its smallest path loss; 3) it is worth noting that NNFF has higher outage probability than RNRF in non-cooperative NOMA, however, it achieves lower outage probability than RNRF in cooperative NOMA. This phenomenon indicates that it is very helpful and necessary to apply cooperative NOMA in NNFF due to the largest performance gain over non-cooperative NOMA.

C. Throughput in Delay-Sensitive Transmission Mode

Fig. 8 plots the system throughput versus SNR with different targeted rates. One can observe that NNNF achieves the highest throughput since it has the lowest outage probability among three selection schemes. The figure also demonstrates the existence of the throughput ceilings in the high SNR region. This is due to the fact that the outage probability is approaching zero and the throughput is determined only by the targeted data rate. It is worth noting that increasing

[1]It is common to use outage probability as a criterion to compare the performance of cooperative transmission and non-cooperative transmission schemes [14]. In the context of cooperative NOMA, the use of outage probability is particularly useful since the purpose of cooperative NOMA is to improve the reception reliability of the far users.

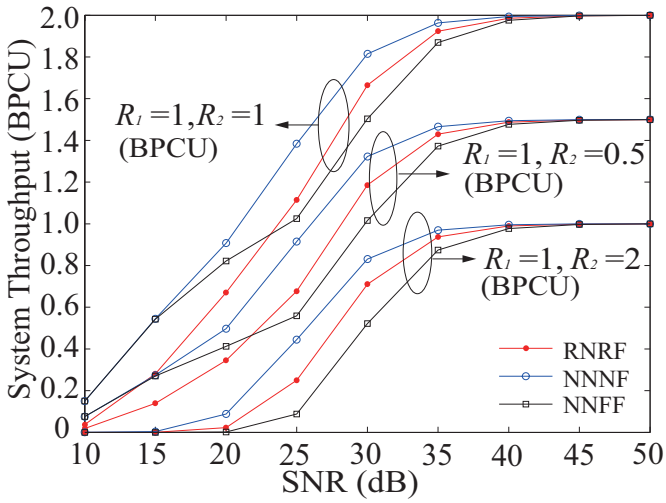

Fig. 8. System throughput in delay-sensitive mode versus SNR with different rate, $\alpha = 2$, $R_{D_A} = 10\ m$, $R_{D_B} = 2\ m$, $R_{D_C} = 8\ m$, $\lambda_{\Phi_A} = 1$, and $\lambda_{\Phi_B} = 1$.

R_2 from $R_2 = 0.5$ BPCU to $R_2 = 1$ BPCU can improve the throughput; however, for the case $R_2 = 2$ BPCU, the throughput is lowered. This is because, in the latter case, the energy remaining for information decoding is not sufficient for message detection of the near user, and hence an outage occurs, which in turn affects the throughput. Therefore, we see that it is important to select appropriate transmission rates when designing practical NOMA downlink transmission systems.

V. Conclusions

In this paper, the application of SWIPT to NOMA has been considered. A novel cooperative SWIPT NOMA protocol with three different user selection criteria has been

proposed. We have used the stochastic geometric approach to provide a complete framework to model the locations of users and evaluate the performance of the proposed user selection schemes. Closed-form results have been derived in terms of outage probability and delay-sensitive throughput to determine the system performance. The diversity gain of the three user selection schemes has also been characterized and proved to be the same as that of a conventional cooperative network. For the proposed protocol, the decreasing rate of the outage probability of far users is $\frac{\ln SNR}{SNR^2}$ while it is $\frac{1}{SNR^2}$ for a conventional cooperative network. Numerical results have been presented to validate our analysis. We conclude that by carefully choosing the parameters of the network, (e.g., transmission rate or power splitting coefficient), acceptable system performance can be guaranteed even if the users do not use their own batteries to power the relay transmission.

Appendix A: Proof of Theorem 2

Substituting (4) and (12) into (22), the outage probability can be expressed as follows:

$$P_{\mathrm{A_i}} = \underbrace{\Pr\left(\gamma_{\mathrm{A_i,MRC}}^{x_{i1}} < \tau_1, \frac{\rho|h_{\mathrm{B_i}}|^2|p_{i1}|^2}{\rho|h_{\mathrm{B_i}}|^2|p_{i2}|^2+1+d_{\mathrm{B_i}}^{\alpha}} > \tau_1\right)}_{\Theta_1} + \underbrace{\Pr\left(\gamma_{\mathrm{S,A_i}}^{x_{i1}} < \tau_1, \frac{\rho|h_{\mathrm{B_i}}|^2|p_{i1}|^2}{\rho|h_{\mathrm{B_i}}|^2|p_{i2}|^2+1+d_{\mathrm{B_i}}^{\alpha}} < \tau_1\right)}_{\Theta_2}, \tag{A.1}$$

We express Θ_1 as (A.2) on the top of next page where $f_{X_i}(x) = \left(1+d_{\mathrm{A_i}}^{\alpha}\right) e^{-\left(1+d_{\mathrm{A_i}}^{\alpha}\right)x}$, and $f_{Y_i}(y) = \left(1+d_{\mathrm{B_i}}^{\alpha}\right) e^{-\left(1+d_{\mathrm{B_i}}^{\alpha}\right)y}$.

Based on (A.2), using $t = y - \varepsilon_{\mathrm{A}_i}$, we calculate Ξ as follows:

$$\Xi = \int_0^{\infty} \left(1 - e^{-\left(1+d_{\mathrm{C_i}}^{\alpha}\right)\frac{\tau - \frac{\rho x|p_{i1}|^2}{\rho x|p_{i2}|^2+1}}{\eta\rho t}}\right) \times \left(1+d_{\mathrm{B_i}}^{\alpha}\right) e^{-\left(1+d_{\mathrm{B_i}}^{\alpha}\right)\left(t+\varepsilon_{\mathrm{A}_i}\right)} dt. \tag{A.3}$$

Applying [15, Eq. (3.324)], we rewrite (A.3) as follows:

$$\Xi = e^{-\left(1+d_{\mathrm{B_i}}^{\alpha}\right)\varepsilon_{\mathrm{A}_i}} \left(1 - 2\sqrt{\chi\Lambda}K_1\left(2\sqrt{\chi\Lambda}\right)\right), \tag{A.4}$$

where $\Lambda = \frac{\left(1+d_{\mathrm{B_i}}^{\alpha}\right)\left(1+d_{\mathrm{C_i}}^{\alpha}\right)}{\eta\rho}$ and $\chi = \tau_1 - \frac{\rho x|p_{i1}|^2}{\rho x|p_{i2}|^2+1}$.

We use the series representation of Bessel functions to obtain the high SNR approximation which is expressed as follows:

$$xK_1(x) \approx 1 + \frac{x^2}{2}\left(\ln\frac{x}{2} + c_0\right), \tag{A.5}$$

where $K_1(\cdot)$ is the modified Bessel function for the seconde kind, $c_0 = -\frac{\varphi(1)}{2} - \frac{\varphi(2)}{2}$, and $\varphi(\cdot)$ denotes the psi function [15].

To obtain the high SNR approximation of (A.4) and using (A.5), we obtain

$$\Xi \approx -\chi\Lambda\left(\ln\chi\Lambda + 2c_0\right). \tag{A.6}$$

Substituting (A.6) into (A.2), we rewrite (A.2) as follows:

$$\Theta_1 = -\int_0^{\varepsilon_{\mathrm{A}_i}} \chi \int_{D_{\mathrm{A_i}}} \Lambda e^{-\left(1+d_{\mathrm{A_i}}^{\alpha}\right)x} \times \underbrace{\int_{D_{\mathrm{B_i}}} \left(1+d_{\mathrm{B_i}}^{\alpha}\right)\left(\ln\chi\Lambda + 2c_0\right) f_{W_{\mathrm{B_i}}}(\omega_{\mathrm{B_i}})\, d\omega_{\mathrm{B_i}}}_{\Phi} f_{W_{\mathrm{A_i}}}(\omega_{\mathrm{A_i}})\, d\omega_{\mathrm{A_i}} dx. \tag{A.7}$$

Since $d_{\mathrm{C_i}} = \sqrt{d_{\mathrm{A_i}}^2 + d_{\mathrm{B_i}}^2 - 2d_{\mathrm{A_i}}d_{\mathrm{B_i}}\cos(\theta_i)}$ and $R_{D_{\mathrm{C}}} \gg R_{D_{\mathrm{B}}}$, we can approximate the distance as $d_{\mathrm{A_i}} \approx d_{\mathrm{C_i}}$. Applying (16), we calculate Φ as follows:

$$\Phi \approx \frac{2}{R_{D_{\mathrm{B}}}^2}\int_0^{R_{D_{\mathrm{B}}}} \left(1+r^{\alpha}\right)\left(\ln m_0\left(1+r^{\alpha}\right) + 2c_0\right) r dr, \tag{A.8}$$

where $m_0 = \frac{\chi\left(1+d_{\mathrm{C_i}}^{\alpha}\right)}{\eta\rho} \approx \frac{\chi\left(1+d_{\mathrm{A_i}}^{\alpha}\right)}{\eta\rho}$.

For an arbitrary choice of α, the integral in (A.8) is mathematically intractable, we use Gaussian-Chebyshev quadrature to find the approximation. Then Φ can be approximated as follows:

$$\Phi \approx \frac{\omega_N}{2}\sum_{n=1}^{N}\left(\sqrt{1-\phi_n{}^2}c_n\left(\ln m_0 c_n + 2c_0\right)\left(\phi_n+1\right)\right). \tag{A.9}$$

Substituting (A.9) into (A.7), we rewrite (A.7) as follows:

$$\Theta_1 = -\frac{\omega_N}{R_{D_{\mathrm{A}}}^2 - R_{D_{\mathrm{C}}}^2}\int_0^{\varepsilon_{\mathrm{A}_i}} \frac{\chi}{\eta\rho}\sum_{n=1}^{N}\left(\phi_n+1\right)\sqrt{1-\phi_n{}^2} \underbrace{\int_{R_{D_{\mathrm{C}}}}^{R_{D_{\mathrm{A}}}} r(1+r^{\alpha})^2 e^{-(1+r^{\alpha})x} c_n\left(\ln\frac{\chi\left(1+r^{\alpha}\right)}{\eta\rho}c_n + 2c_0\right) dr}_{\Delta} dx. \tag{A.10}$$

Similarly as above, we use Gaussian-Chebyshev quadrature to find an approximation of Δ in (A.10) as follows:

$$\Delta \approx \frac{\omega_K\left(R_{D_{\mathrm{A}}} - R_{D_{\mathrm{C}}}\right)}{2}\sum_{k=1}^{K}\sqrt{1-\psi_k^2}s_k(1+s_k^{\alpha})^2 \times e^{-(1+s_k^{\alpha})x} c_n\left(\ln\frac{\chi\left(1+s_k^{\alpha}\right)}{\eta\rho}c_n + 2c_0\right). \tag{A.11}$$

Substituting (A.11) into (A.10), we rewrite (A.10) as follows:

$$\Theta_1 = a_2\sum_{n=1}^{N}\left(\phi_n+1\right)\sqrt{1-\phi_n{}^2}c_n\sum_{k=1}^{K}\sqrt{1-\psi_k^2}s_k(1+s_k^{\alpha})^2 \times \underbrace{\int_0^{\varepsilon_{\mathrm{A}_i}} \chi e^{-(1+s_k^{\alpha})x}\left(\ln\frac{\chi\left(1+s_k^{\alpha}\right)}{\eta\rho}c_n + 2c_0\right) dx}_{\Psi}, \tag{A.12}$$

where $a_2 = -\frac{\omega_N\omega_K}{2\left(R_{D_{\mathrm{A}}}+R_{D_{\mathrm{C}}}\right)\eta\rho}$.

$$\Theta_1 = \Pr\left(Z_i < \frac{\tau_1 - \frac{\rho X_i |p_{i1}|^2}{\rho X_i |p_{i2}|^2 + 1}}{\eta\rho\left(Y_i - \varepsilon_{\mathrm{A}_i}\right)}, X_i < \varepsilon_{\mathrm{A}_i}, Y_i > \varepsilon_{\mathrm{A}_i}\right)$$
$$= \int_{D_\mathrm{B}}\int_{D_\mathrm{A}}\int_0^{\varepsilon_{\mathrm{A}_i}} \underbrace{\int_{\varepsilon_{\mathrm{A}_i}}^{\infty}\left(1 - e^{-\left(1+d_{\mathrm{C_i}}^{\alpha}\right)\frac{\tau_1 - \frac{\rho x |p_{i1}|^2}{\rho x |p_{i2}|^2 + 1}}{\eta\rho\left(y - \varepsilon_{\mathrm{A}_i}\right)}}\right) f_{Y_i}(y)\, dy}_{\Xi} f_{X_i}(x)\, dx f_{W_{\mathrm{A_i}}}(\omega_{\mathrm{A_i}})\, d\omega_{\mathrm{A_i}} f_{W_{\mathrm{B_i}}}(\omega_{\mathrm{B_i}})\, d\omega_{\mathrm{B_i}}, \tag{A.2}$$

Similarly, we use Gaussian-Chebyshev quadrature to find an approximation of Ψ in (A.12) as follows:

$$\Psi \approx \frac{\omega_M \varepsilon_{\mathrm{A}_i}}{2}\sum_{m=1}^{M}\sqrt{1-\varphi_m^2}\, e^{-(1+s_k^{\alpha})t_m} \times \chi_{t_m}\left(\ln\frac{\chi_{t_m}\left(1+s_k^{\alpha}\right)}{\eta\rho}c_n + 2c_0\right). \tag{A.13}$$

Substituting (A.13) into (A.12), we obtain

$$\Theta_1 \approx \zeta_1 \sum_{n=1}^{N}\left(\phi_n + 1\right)\sqrt{1-{\phi_n}^2}\, c_n \sum_{k=1}^{K}\sqrt{1-\psi_k^2}\, s_k (1+s_k^{\alpha})^2 \sum_{m=1}^{M}\sqrt{1-\varphi_m^2}\, e^{-(1+s_k^{\alpha})t_m}\chi_{t_m}\left(\ln\frac{\chi_{t_m}\left(1+s_k^{\alpha}\right)}{\eta\rho}c_n + 2c_0\right). \tag{A.14}$$

We express Θ_2 as follows:

$$\Theta_2 = \Pr\left(X_i < \varepsilon_{\mathrm{A}_i}\right)\Pr\left(Y_i < \varepsilon_{\mathrm{A}_i}\right). \tag{A.15}$$

The CDF of X_i for $\mathrm{A_i}$ is given by

$$F_{X_i}(\varepsilon) = \int_D\left(1 - e^{-\left(1+d_{\mathrm{A_i}}^{\alpha}\right)\varepsilon}\right) f_{W_{\mathrm{A_i}}}(\omega_{\mathrm{A_i}})\, d\omega_{\mathrm{A_i}} = \frac{2}{R_{D_\mathrm{A}}^2 - R_{D_\mathrm{C}}^2}\int_{R_{D_\mathrm{C}}}^{R_{D_\mathrm{A}}}\left(1 - e^{-(1+r^{\alpha})\varepsilon}\right) r dr. \tag{A.16}$$

For an arbitrary choice of α, similarly to (19), we provide Gaussian-Chebyshev quadrature to find the approximation for the CDF of X_i. We rewrite (A.16) as follows:

$$F_{X_i}(\varepsilon) \approx \frac{\omega_K}{R_{D_\mathrm{A}} + R_{D_\mathrm{C}}}\sum_{k=1}^{K}\sqrt{1-{\psi_k}^2}\left(1 - e^{-(1+s_k^{\alpha})\varepsilon}\right) s_k. \tag{A.17}$$

When $\varepsilon \to 0$, a high SNR approximation of the (A.17) is given by

$$F_{X_i}(\varepsilon) \approx \frac{\omega_K \varepsilon}{R_{D_\mathrm{A}} + R_{D_\mathrm{C}}}\sum_{k=1}^{K}\sqrt{1-{\psi_k}^2}(1+s_k^{\alpha}) s_k. \tag{A.18}$$

Substituting (A.18) and (19) into (A.15), we can obtain the approximation for the general case as follows:

$$\Theta_2 \approx a_1 \sum_{n=1}^{N}\sqrt{1-{\phi_n}^2}\, c_n\left(\phi_n + 1\right)\sum_{k=1}^{K}\sqrt{1-{\psi_k}^2}(1+s_k^{\alpha}) s_k. \tag{A.19}$$

Combining (A.14) and (A.19), we can obtain (23).
The proof is completed.

Appendix B: Proof of Corollary 2

For the special case $\alpha = 2$, and let $\lambda = \left(1 + r^2\right)$, we rewrite (A.8) as follows:

$$\Phi|_{\alpha=2} = \frac{1}{R_{D_\mathrm{B}}^2}\int_1^{1+R_{D_\mathrm{B}}^2}\lambda\left(\ln m_{0^*}\lambda + 2c_0\right) d\lambda = \frac{\left(R_{D_\mathrm{B}}^2 + 2\right)\ln m_{0^*}}{2} + b_0, \tag{B.1}$$

where $m_{0^*} = \frac{\chi\left(1+d_{\mathrm{C_i}}^2\right)}{\eta\rho} \approx \frac{\chi\left(1+d_{\mathrm{A_i}}^2\right)}{\eta\rho}$.
Substituting (B.1) and applying $\alpha = 2$ into (A.2), we obtain

$$\Theta_1|_{\alpha=2} = -\frac{\left(R_{D_\mathrm{B}}^2 + 2\right)}{2\left(R_{D_\mathrm{A}}^2 - R_{D_\mathrm{C}}^2\right)\eta\rho}\int_0^{\varepsilon_{\mathrm{A}_i}}\chi \underbrace{\int_{R_{D_\mathrm{C}}}^{R_{D_\mathrm{A}}} r\left(1+r^2\right)^2 e^{-(1+r^2)x}\left(\ln\frac{\chi\left(1+r^2\right)}{\eta\rho} + b_0\right) dr}_{\Delta|_{\alpha=2}} dx. \tag{B.2}$$

We notice that the integral $\Delta|_{\alpha=2}$ in (B.2) is mathematically intractable. We use Gaussian-Chebyshev quadrature to find an approximation. Then $\Delta|_{\alpha=2}$ can be approximated as follows:

$$\Delta|_{\alpha=2} \approx \frac{\omega_K\left(R_{D_\mathrm{A}} - R_{D_\mathrm{C}}\right)}{2}\sum_{k=1}^{K}\sqrt{1-\psi_k^2}\, s_k\left(1+s_k^2\right)^2 e^{-\left(1+s_k^2\right)x}\left(\ln\frac{\chi\left(1+s_k^2\right)}{\eta\rho} + b_0\right). \tag{B.3}$$

Substituting (B.3) into (B.2), we rewrite (B.2) as follows:

$$\Theta_1|_{\alpha=2} = -\frac{\omega_K\left(R_{D_\mathrm{B}}^2 + 2\right)}{4\left(R_{D_\mathrm{A}} + R_{D_\mathrm{C}}\right)\eta\rho}\sum_{k=1}^{K}\sqrt{1-\psi_k^2}\, s_k\left(1+s_k^2\right)^2 \times \underbrace{\int_0^{\varepsilon_{\mathrm{A}_i}}\chi e^{-\left(1+s_k^2\right)x}\left(\ln\frac{\chi\left(1+s_k^2\right)}{\eta\rho} + b_0\right) dx}_{\Psi|_{\alpha=2}}. \tag{B.4}$$

Similarly, we use Gaussian-Chebyshev quadrature to find the approximation of $\Psi|_{\alpha=2}$ in (B.4) as follows:

$$\Psi|_{\alpha=2} \approx \frac{\omega_M \varepsilon_{\mathrm{A}_i}}{2}\sum_{m=1}^{M}\sqrt{1-\varphi_m^2} \times \chi_{t_m} e^{-\left(1+s_k^2\right)t_m}\left(\ln\frac{\chi_{t_m}\left(1+s_k^2\right)}{\eta\rho}c_n + b_0\right). \tag{B.5}$$

Substituting (B.5) into (B.4), we obtain

$$\Theta_1|_{\alpha=2} = \zeta_2 \sum_{k=1}^{K} \sqrt{1-\psi_k^2} s_k \left(1+s_k^2\right)^2 \sum_{m=1}^{M} \sqrt{1-\varphi_m^2} \times \chi_{t_m} e^{-\left(1+s_k^2\right)t_m} \left(\ln \frac{\chi_{t_m}\left(1+s_k^2\right)}{\eta\rho} c_n + b_0 \right). \quad \text{(B.6)}$$

For the special case $\alpha = 2$, the CDF of X_i in (A.16) can be calculated as follows:

$$F_{X_i}(\varepsilon)|_{\alpha=2} = 1 - \frac{e^{-\left(1+R_{D_\mathrm{C}}^2\right)\varepsilon}}{\varepsilon\left(R_{D_\mathrm{A}}^2 - R_{D_\mathrm{C}}^2\right)} + \frac{e^{-\left(1+R_{D_\mathrm{A}}^2\right)\varepsilon}}{\varepsilon\left(R_{D_\mathrm{A}}^2 - R_{D_\mathrm{C}}^2\right)}. \quad \text{(B.7)}$$

Substituting (B.7) and (21) into (A.15), we can obtain Θ_2 for the special case $\alpha = 2$ in exact closed-form as follows:

$$\Theta_2|_{\alpha=2} = \left(1 - \frac{e^{-\left(1+R_{D_\mathrm{C}}^2\right)\varepsilon_{\mathrm{A}_i}}}{\varepsilon_{\mathrm{A}_i}\left(R_{D_\mathrm{A}}^2 - R_{D_\mathrm{C}}^2\right)} + \frac{e^{-\left(1+R_{D_\mathrm{A}}^2\right)\varepsilon_{\mathrm{A}_i}}}{\varepsilon_{\mathrm{A}_i}\left(R_{D_\mathrm{A}}^2 - R_{D_\mathrm{C}}^2\right)}\right) \times \left(1 - \frac{e^{-\varepsilon_{\mathrm{A}_i}}}{R_{D_\mathrm{B}}^2\varepsilon_{\mathrm{A}_i}} + \frac{e^{-\left(1+R_{D_\mathrm{B}}^2\right)\varepsilon_{\mathrm{A}_i}}}{R_{D_\mathrm{B}}^2\varepsilon_{\mathrm{A}_i}}\right). \quad \text{(B.8)}$$

Combining (B.6) and (B.8), we can obtain (24).

The proof is completed.

Appendix C: Proof of Theorem 4

Conditioned on the event that the numbers of users in group $\{\mathrm{A_i}\}$ and $\{\mathrm{B_i}\}$ satisfy $\mathrm{V} = N_\mathrm{A} \geq 1, N_\mathrm{B} \geq 1$, we express the outage probability for A_{i^*} by applying $X_{i^*} \to X_i$, $Y_{i^*} \to Y_i$, and $Z_{i^*} \to Z_i$ in (A.1) then obtain

$$P_{\mathrm{A}_{i^*}} = \underbrace{\Pr\left(\frac{\rho X_{i^*}|p_{i1}|^2}{\rho X_{i^*}|p_{i2}|^2+1} < \tau_1, \frac{\rho Y_{i^*}|p_{i1}|^2}{\rho|p_{i2}|^2 Y_{i^*}+1} < \tau_1 \middle| \mathrm{V}\right)}_{\Theta_2^*} + \underbrace{\Pr\left(Z_{i^*} < \frac{\tau_1 - \frac{\rho X_{i^*}|p_{i1}|^2}{\rho X_{i^*}|p_{i2}|^2+1}}{\eta\rho\left(Y_{i^*}-\varepsilon_{\mathrm{A}_i}\right)}, X_{i^*} < \varepsilon_{\mathrm{A}_i}, Y_{i^*} > \varepsilon_{\mathrm{A}_i} \middle| \mathrm{V}\right)}_{\Theta_1^*}, \quad \text{(C.1)}$$

where $X_{i^*} = \frac{|h_{\mathrm{A_i}}|^2}{1+d_{\mathrm{A}_{i^*}}^{\alpha}}$, $Y_{i^*} = \frac{|h_{\mathrm{B_i}}|^2}{1+d_{\mathrm{B}_{i^*}}^{\alpha}}$, and $Z_{i^*} = \frac{|g_i|^2}{1+d_{\mathrm{C}_{i^*}}^{\alpha}}$. Here $d_{\mathrm{A}_{i^*}}$, $d_{\mathrm{B}_{i^*}}$, and $d_{\mathrm{C}_{i^*}}$ are distances from the BS to A_{i^*}, from the BS to B_{i^*}, and from A_{i^*} to B_{i^*}, respectively.

Since $R_{D_\mathrm{C}} \gg R_{D_\mathrm{B}}$, we can approximate the distance as $d_{\mathrm{A}_{i^*}} \approx d_{\mathrm{C}_{i^*}}$. Using a similar approximation method as that used to obtain (A.2), we calculate Θ_1^* as follows:

$$\Theta_1^* = -\int_0^{\varepsilon_{\mathrm{A}_i}} \chi \int_{R_{D_\mathrm{C}}}^{R_{D_\mathrm{A}}} \frac{\left(1+r_\mathrm{A}^{\alpha}\right)^2}{\eta\rho} e^{-(1+r_\mathrm{A}^{\alpha})x} \Phi^* f_{d_{\mathrm{A}_{i^*}}}(r_\mathrm{A})\, dr_\mathrm{A} dx, \quad \text{(C.2)}$$

where $\Phi^* = \int_0^{R_{D_\mathrm{B}}} \left(1+r_\mathrm{B}^{\alpha}\right)\left(\ln \chi \frac{(1+r_\mathrm{B}^{\alpha})(1+r_\mathrm{A}^{\alpha})}{\eta\rho} + 2c_0\right) f_{d_{\mathrm{B}_{i^*}}}(r_\mathrm{B})\, dr_\mathrm{B}$ and $f_{d_{\mathrm{A}_{i^*}}}$ is the PDF of the nearest A_{i^*}.

Similar to (33) and applying stochastic geometry within the ring D_A, we obtain $f_{d_{\mathrm{A}_{i^*}}}(r_\mathrm{A})$ as follows:

$$f_{d_{\mathrm{A}_{i^*}}}(r_\mathrm{A}) = \xi_\mathrm{A} r_\mathrm{A} e^{-\pi\lambda_{\Phi_\mathrm{A}}\left(r_\mathrm{A}^2 - R_{D_\mathrm{C}}^2\right)}, \quad \text{(C.3)}$$

where $\xi_\mathrm{A} = \frac{2\pi\lambda_{\Phi_\mathrm{A}}}{1-e^{-\pi\lambda_{\Phi_\mathrm{A}}\left(R_{D_\mathrm{A}}^2 - R_{D_\mathrm{C}}^2\right)}}$.

Substituting (C.3) and (33) into (C.2), and using the Gaussian-Chebyshev quadrature approximation, Φ^* can be expressed as follows:

$$\Phi^* \approx \frac{\xi_\mathrm{B}\omega_N R_{D_\mathrm{B}}}{2} \sum_{n=1}^{N} \sqrt{1-\phi_n^2}\left(1+c_{n*}^{\alpha}\right) \times \left(\ln m_{\mathrm{B}*}\left(1+c_{n*}^{\alpha}\right) + 2c_0\right) c_{n*} e^{-\pi\lambda_{\Phi_\mathrm{B}} c_{n*}^2}. \quad \text{(C.4)}$$

where $m_{\mathrm{B}*} = \frac{\chi(1+r_\mathrm{A}^{\alpha})}{\eta\rho}$.

Substituting (C.4) into (C.2), we obtain

$$\Theta_1^* = -\frac{\xi_\mathrm{B}\xi_\mathrm{A}\omega_N R_{D_\mathrm{B}}}{2\eta\rho} \int_0^{\varepsilon_{\mathrm{A}_i}} \chi e^{-(1+r_\mathrm{A}^{\alpha})x} \times \sum_{n=1}^{N} \sqrt{1-\phi_n^2}\left(1+c_{n*}^{\alpha}\right) c_{n*} e^{-\pi\lambda_{\Phi_\mathrm{B}} c_{n*}^2} \Delta^* dx, \quad \text{(C.5)}$$

where $\Delta^* = \int_{R_{D_\mathrm{C}}}^{R_{D_\mathrm{A}}} \left(\ln \chi \frac{(1+r_\mathrm{A}^{\alpha})}{\eta\rho}\left(1+c_{n*}^{\alpha}\right) + 2c_0\right) \times \left(1+r_\mathrm{A}^{\alpha}\right)^2 r_\mathrm{A} e^{-\pi\lambda_{\Phi_\mathrm{A}}\left(r_\mathrm{A}^2 - R_{D_\mathrm{C}}^2\right)} dr_\mathrm{A}$.

Applying Gaussian-Chebyshev quadrature approximation to Δ^*, we obtain

$$\Delta^* \approx \frac{\omega_K\left(R_{D_\mathrm{A}} - R_{D_\mathrm{C}}\right)}{2} \sum_{k=1}^{K} \sqrt{1-\psi_k^2}\left(1+s_k^{\alpha}\right)^2 \times \left(\ln \frac{\chi\left(1+s_k^{\alpha}\right)\left(1+c_{n*}^{\alpha}\right)}{\eta\rho} + 2c_0\right) s_k e^{-\pi\lambda_{\Phi_\mathrm{A}}\left(s_k^2 - R_{D_\mathrm{C}}^2\right)}. \quad \text{(C.6)}$$

Substituting (C.6) into (C.2), we obtain

$$\Theta_1^* = b_5 \sum_{n=1}^{N} \sqrt{1-\phi_n^2}\left(1+c_{n*}^{\alpha}\right) c_{n*} e^{-\pi\lambda_{\Phi_\mathrm{B}} c_{n*}^2} \times \sum_{k=1}^{K} \sqrt{1-\psi_k^2}\left(1+s_k^{\alpha}\right)^2 s_k e^{-\pi\lambda_{\Phi_\mathrm{A}}\left(s_k^2 - R_{D_\mathrm{C}}^2\right)} \times \underbrace{\int_0^{\varepsilon_{\mathrm{A}_i}} \chi e^{-(1+r_\mathrm{A}^{\alpha})x} \left(\ln \frac{\chi\left(1+s_k^{\alpha}\right)\left(1+c_{n*}^{\alpha}\right)}{\eta\rho} + 2c_0\right) dx}_{\Psi^*}, \quad \text{(C.7)}$$

where $b_5 = -\frac{\xi_\mathrm{B}\xi_\mathrm{A}\omega_N\omega_K R_{D_\mathrm{B}}\left(R_{D_\mathrm{A}} - R_{D_\mathrm{C}}\right)}{4\eta\rho}$.

Applying Gaussian-Chebyshev quadrature approximation to Ψ^*, we obtain

$$\Psi^* \approx \sum_{m=1}^{M} \omega_M \frac{\varepsilon_{\mathrm{A}_i}}{2} \sqrt{1-\varphi_m^2} e^{-(1+s_k^{\alpha})t_m} \times \chi_{t_m}\left(\ln \frac{\chi_{t_m}\left(1+s_k^{\alpha}\right)\left(1+c_{n*}^{\alpha}\right)}{\eta\rho} + 2c_0\right). \quad \text{(C.8)}$$

Substituting (C.8) into (C.7), we obtain

$$\Theta_1^* = \varsigma^* \sum_{n=1}^{N} \sqrt{1-\phi_n{}^2}\,(1+c_{n*}^{\alpha})\,c_{n*} e^{-\pi\lambda_{\Phi_{\mathrm{B}}} c_{n*}^2} \sum_{k=1}^{K} \sqrt{1-\psi_k^2} \times (1+s_k^{\alpha})^2 s_k e^{-\pi\lambda_{\Phi_{\mathrm{A}}}\left(s_k^2 - R_{D_{\mathrm{C}}}^2\right)} \sum_{m=1}^{M} \sqrt{1-\varphi_m^2} \times e^{-(1+s_k^{\alpha})t_m} \chi_{t_m} \left(\ln \frac{\chi_{t_m}\,(1+s_k^{\alpha})\,(1+c_{n*}^{\alpha})}{\eta\rho} + 2c_0\right). \tag{C.9}$$

Conditioned on the number of users in group $\{\mathrm{A_i}\}$ and $\{\mathrm{B_i}\}$, we obtain Θ_2^* as follows:

$$\begin{aligned}\Theta_2^* &= \Pr\left(X_{i^*} < \varepsilon_{\mathrm{A}_i} \middle| N_{\mathrm{A}} \geq 1\right) \Pr\left(Y_{i^*} < \varepsilon_{\mathrm{A}_i} \middle| N_{\mathrm{B}} \geq 1\right) \\ &= F_{X_{i^*}}\left(\varepsilon_{\mathrm{A}_i}\right) F_{Y_{i^*}}\left(\varepsilon_{\mathrm{A}_i}\right).\end{aligned} \tag{C.10}$$

Similar to (34), the CDF of $\mathrm{A_{i^*}}$ is given by

$$\begin{aligned}&F_{X_{i^*}}(\varepsilon) \\ &= \xi_{\mathrm{A}} \int_{R_{D_{\mathrm{C}}}}^{R_{D_{\mathrm{A}}}} \left(1 - e^{-(1+r_{\mathrm{A}}^{\alpha})\varepsilon}\right) r_{\mathrm{A}} e^{-\pi\lambda_{\Phi_{\mathrm{A}}}\left(r_{\mathrm{A}}^2 - R_{D_{\mathrm{C}}}^2\right)} dr_{\mathrm{A}}.\end{aligned} \tag{C.11}$$

Applying the Gaussian-Chebyshev quadrature approximation, we obtain

$$F_{X_{i^*}}(\varepsilon) \approx b_2 \sum_{k=1}^{K} \sqrt{1-\psi_k{}^2} \left(1 - e^{-(1+s_k^{\alpha})\varepsilon}\right) s_k e^{-\pi\lambda_{\Phi_{\mathrm{A}}} s_k^2}. \tag{C.12}$$

Substituting (C.12) and (35) into (C.10) and using a high SNR approximation, we obtain

$$\begin{aligned}\Theta_2^* \approx & b_2 b_3 \sum_{k=1}^{K} \sqrt{1-\psi_k{}^2}(1+s_k^{\alpha}) s_k e^{-\pi\lambda_{\Phi_{\mathrm{A}}} s_k^2} \\ & \times \sum_{n=1}^{N} \left(\sqrt{1-\phi_n{}^2}\,(1+c_{n*}^{\alpha})\,c_{n*} e^{-\pi\lambda_{\Phi_{\mathrm{B}}} c_{n*}^2}\right).\end{aligned} \tag{C.13}$$

Combining (C.13) and (C.7), we obtain (37).

The proof is completed.

Appendix D: Proof of Theorem 5

We express the outage probability for $\mathrm{A_{i'}}$ by applying $X_{i^*} \to X_i$, $Y_{i^*} \to Y_i$, and $Z_{i^*} \to Z_i$ in (A.1) and obtain

$$\begin{aligned}P_{\mathrm{A}_{i'}} = & \underbrace{\Pr\left(\frac{\rho X_{i'}|p_{i1}|^2}{\rho X_{i'}|p_{i2}|^2+1} < \tau_1, \frac{\rho Y_{i^*}|p_{i1}|^2}{\rho|p_{i2}|^2 Y_{i^*}+1} < \tau_1 \middle| \mathrm{V}\right)}_{\Theta_2{}'} \\ & + \underbrace{\Pr\left(Z_{i'} < \frac{\tau_1 - \frac{\rho X_{i'}|p_{i1}|^2}{\rho X_{i'}|p_{i2}|^2+1}}{\eta\rho\left(Y_{i^*} - \varepsilon_{\mathrm{A}_i}\right)}, X_{i'} < \varepsilon_{\mathrm{A}_i}, Y_{i^*} > \varepsilon_{\mathrm{A}_i} \middle| \mathrm{V}\right)}_{\Theta_1{}'},\end{aligned} \tag{D.1}$$

where $X_{i'} = \frac{|h_{\mathrm{A}_i}|^2}{1+d_{\mathrm{A}_{i'}}^{\alpha}}$ and $Z_{i'} = \frac{|g_i|^2}{1+d_{\mathrm{C}_{i'}}^{\alpha}}$. Here $d_{\mathrm{A}_{i'}}$ and $d_{\mathrm{C}_{i'}}$ are distances from the BS to $\mathrm{A_{i'}}$ and from $\mathrm{A_{i'}}$ to $\mathrm{B_{i^*}}$, respectively.

Since $R_{D_{\mathrm{C}}} \gg R_{D_{\mathrm{B}}}$, we can approximate the distance as $d_{\mathrm{A}_{i'}} \approx d_{\mathrm{C}_{i'}}$. Using a similar approximation method as that used to get (A.2), we first calculate $\Theta_1{}'$ as follows:

$$\begin{aligned}\Theta_1{}' = & -\int_0^{\varepsilon_{\mathrm{A}_i}} \chi \int_{R_{D_C}}^{R_{D_{\mathrm{A}}}} \frac{(1+r_{\mathrm{A}}^{\alpha})^2}{\eta\rho} e^{-(1+r_{\mathrm{A}}^{\alpha})x} \\ & \times \int_0^{R_{D_{\mathrm{B}}}} (1+r_{\mathrm{B}}^{\alpha}) \left(\ln \chi \frac{(1+r_{\mathrm{B}}^{\alpha})\,(1+r_{\mathrm{A}}^{\alpha})}{\eta\rho} + 2c_0\right) \\ & \times f_{d_{\mathrm{B}_{i^*}}}(r_{\mathrm{B}})\,dr_{\mathrm{B}} f_{d_{\mathrm{A}_{i'}}}(r_{\mathrm{A}})\,dr_{\mathrm{A}}dx,\end{aligned} \tag{D.2}$$

where $f_{d_{\mathrm{A}_{i'}}}(r_{\mathrm{A}})$ is the PDF for the farthest $\mathrm{A_{i'}}$.

Similar to (33) and applying stochastic geometry within the ring D_{A}, we can obtain $f_{d_{\mathrm{A}_{i'}}}(r_{\mathrm{A}})$ as follows:

$$f_{d_{\mathrm{A}_{i'}}}(r_{\mathrm{A}}) = \xi_{\mathrm{A}} r_{\mathrm{A}} e^{-\pi\lambda_{\Phi_{\mathrm{A}}}\left(R_{D_{\mathrm{A}}}^2 - r_{\mathrm{A}}^2\right)}. \tag{D.3}$$

Conditioned on the number of $\mathrm{A_{i'}}$ and $\mathrm{B_{i^*}}$, we obtain

$$\begin{aligned}\Theta_2{}' &= \Pr\left(X_{i'} < \varepsilon_{\mathrm{A}_i} \middle| N_{\mathrm{A}} \geq 1\right) \Pr\left(Y_{i^*} < \varepsilon_{\mathrm{A}_i} \middle| N_{\mathrm{B}} \geq 1\right) \\ &= F_{X_{i'}}\left(\varepsilon_{\mathrm{A}_i}\right) F_{Y_{i^*}}\left(\varepsilon_{\mathrm{A}_i}\right).\end{aligned} \tag{D.4}$$

Following a similar procedure as that used to obtain Θ_1^* and Θ_2^* in Appendix B, we can obtain $\Theta_1{}'$ and $\Theta_2{}'$. Then combining $\Theta_1{}'$ and $\Theta_2{}'$, the general case (42) is obtained. For the special case $\alpha = 2$, following a method similar to that used to calculate (38), we can obtain (43).

The proof is completed.

References

[1] Y. Saito, A. Benjebbour, Y. Kishiyama, and T. Nakamura, "System-level performance evaluation of downlink non-orthogonal multiple access (NOMA)," in *Proc. IEEE Annual Symposium on Personal, Indoor and Mobile Radio Communications (PIMRC)*, London, UK, Sept. 2013.

[2] Z. Ding, P. Fan, and H. V. Poor, "Impact of user pairing on 5G non-orthogonal multiple access," *IEEE Trans. Veh. Technol.*, to appear in 2015.

[3] Z. Ding, Z. Yang, P. Fan, and H. V. Poor, "On the performance of non-orthogonal multiple access in 5G systems with randomly deployed users," *IEEE Signal Process. Lett.*, vol. 21, no. 12, pp. 1501–1505, 2014.

[4] M. Al-Imari, P. Xiao, M. A. Imran, and R. Tafazolli, "Uplink non-orthogonal multiple access for 5G wireless networks," in *Proc. of the 11th International Symposium on Wireless Communications Systems (ISWCS)*, Barcelona, Spain, Aug 2014, pp. 781–785.

[5] Z. Ding, M. Peng, and H. V. Poor, "Cooperative non-orthogonal multiple access in 5G systems," *IEEE Commun. Lett.*, vol. 19, no. 8, pp. 1462–1465, 2015.

[6] L. Varshney, "Transporting information and energy simultaneously," in *Proc. IEEE Int. Symp. Inf. Theory (ISIT)*, Toronto, ON, 2008, pp. 1612–1616.

[7] R. Zhang and C. K. Ho, "MIMO broadcasting for simultaneous wireless information and power transfer," *IEEE Trans. Commun.*, vol. 12, no. 5, pp. 1989–2001, 2013.

[8] A. A. Nasir, X. Zhou, S. Durrani, and R. A. Kennedy, "Relaying protocols for wireless energy harvesting and information processing," *IEEE Trans. Wireless Commun.*, vol. 12, no. 7, pp. 3622–3636, 2013.

[9] I. Krikidis, S. Sasaki, S. Timotheou, and Z. Ding, "A low complexity antenna switching for joint wireless information and energy transfer in MIMO relay channels," *IEEE Trans. Commun.*, vol. 62, no. 5, pp. 1577–1587, 2014.

[10] Z. Ding, I. Krikidis, B. Sharif, and H. V. Poor, "Wireless information and power transfer in cooperative networks with spatially random relays," *IEEE Trans. Wireless Commun.*, vol. 13, no. 8, pp. 4440–4453, 2014.

[11] Z. Ding and H. Poor, "Cooperative energy harvesting networks with spatially random users," *IEEE Signal Process. Lett.*, vol. 20, no. 12, pp. 1211–1214, Dec 2013.

[12] T. M. Cover and J. A. Thomas, "Elements of information theory," 6th edited, Wiley and Sons, New York, 1991.

[13] E. Hildebrand, "Introduction to Numerical Analysis," New York, USA: Dover,1987.

[14] J. N. Laneman, D. N. Tse, and G. W. Wornell, "Cooperative diversity in wireless networks: Efficient protocols and outage behavior," *IEEE Trans. Inf. Theory*, vol. 50, no. 12, pp. 3062–3080, 2004.

[15] I. S. Gradshteyn and I. M. Ryzhik, *Table of Integrals, Series and Products*, 6th ed. New York, NY, USA: Academic Press, 2000.